

Molecular Dynamics Force Probe Simulations of Antibody/Antigen Unbinding: Entropic Control and Nonadditivity of Unbinding Forces

Berthold Heymann and Helmut Grubmüller

Theoretical Molecular Biophysics Group, Max Planck Institute for Biophysical Chemistry, 37077 Göttingen, Germany

ABSTRACT Unbinding of a spin-labeled dinitrophenyl (DNP) hapten from the monoclonal antibody AN02 F_{ab} fragment has been studied by force probe molecular dynamics (FPMD) simulations. In our nanosecond simulations, unbinding was enforced by pulling the hapten molecule out of the binding pocket. Detailed inspection of the FPMD trajectories revealed a large heterogeneity of enforced unbinding pathways and a correspondingly large flexibility of the binding pocket region, which exhibited induced fit motions. Principal component analyses were used to estimate the resulting entropic contribution of ~6 kcal/mol to the AN02/DNP-hapten bond. This large contribution may explain the surprisingly large effect on binding kinetics found for mutation sites that are not directly involved in binding. We propose that such “entropic control” optimizes the binding kinetics of antibodies. Additional FPMD simulations of two point mutants in the light chain, Y33F and I96K, provided further support for a large flexibility of the binding pocket. Unbinding forces were found to be unchanged for these two mutants. Structural analysis of the FPMD simulations suggests that, in contrast to free energies of unbinding, the effect of mutations on unbinding forces is generally nonadditive.

INTRODUCTION

Molecular recognition is essential for many biochemical processes and may be realized by highly specific binding of ligands to their receptors. In the immune system, antibodies play a crucial role by recognizing and specifically binding their antigens. Calorimetric, spectroscopic, kinetic, and structural data on antibody/antigen systems have been accumulated (Padlan, 1994). Antibodies are widely used in biotechnology, pharmaceuticals (Dickman, 1998), and as catalysts (Kristensen et al., 1998). For a better understanding of the antigen-binding mechanism insight into its molecular dynamics at the atomic level is essential.

Recent advances in single molecule atomic force microscopy (AFM) and other force probe techniques allow one to study mechanical properties of individual molecules such as the binding forces of protein-ligand complexes (Lee et al., 1994b; Florin et al., 1994; Moy et al., 1994), the enforced unfolding of proteins (Rief et al., 1997a; Kellermayer et al., 1997; Tskhovrebova et al., 1997), or the stiffness of other polymers, such as DNA (Lee et al., 1994a) or polysaccharides (Rief et al., 1997b). Also, and motivating the present work, single-molecule AFM studies on a number of antibody/antigen complexes have been carried out (Hinterdorfer et al., 1996; Dammer et al., 1996; Allen et al., 1997; Ros et al., 1998), and more are under way.

Computer simulations of such AFM experiments (Grubmüller et al., 1996; Konrad and Bolonick, 1996; Rief et al., 1997b; Izrailev et al., 1997; Marrink et al., 1998; Lu et al., 1998; Heymann and Grubmüller, 1999a–c) by means of

“force probe” molecular dynamics (FPMD) simulations can provide models that explain the measured forces in terms of molecular structures, unbinding reaction pathways, and interatomic interactions. They thereby complement single molecular AFM experiments with microscopic interpretations. Such simulations can and have to be validated by computing unbinding forces from the simulations and comparing these with experiments. Such a comparison is complicated by the fact that AFM experiments are typically carried out on a millisecond time scale or slower, whereas MD simulations are currently limited to nanoseconds. Because the unbinding force generally depends on how fast the unbinding is enforced, care has to be taken when relating simulations to experiments (Grubmüller et al., 1996; Izrailev et al., 1997; Marrink et al., 1998).

In a prior publication we reported the computation of unbinding forces of an antibody/hapten complex from nanosecond FPMD simulations (Heymann and Grubmüller, 1999a). In particular, we studied the enforced unbinding of a spin-labeled dinitrophenyl (DNP-SL) hapten from the AN02 antibody. The AN02 antibody is one of 12 monoclonal anti-dinitrophenyl spin-label antibodies that have been characterized in terms of their cDNA sequences and binding constants (Leahy et al., 1988). The AN02 antibody is particularly well-characterized by NMR measurements (Theriault et al., 1991, 1993; Martinez-Yamout and McConnell, 1994) and picosecond MD simulations (Theriault et al., 1993).

To rescale the unbinding forces computed from our AN02 FPMD simulations from the nanosecond simulation time scale to the experimental millisecond time scale (and longer), a scaling model has been developed and applied (Heymann and Grubmüller, 1999a). This model considers both friction and activated processes and makes use of the measured spontaneous dissociation rate for the AN02/DNP-hapten complex and the unbinding length that was estimated

Received for publication 5 January 2001 and in final form 2 May 2001.

Address reprint requests to Helmut Grubmüller, Theoretical Molecular Biophysics Group, Max Planck Institute for Biophysical Chemistry, Am Fassberg 11, 37077 Göttingen, Germany. Tel.: 49-551-201-1763; Fax: 49-551-201-1089; E-mail: hgrubmu@gwdg.de.

© 2001 by the Biophysical Society

0006-3495/01/09/1295/19 \$2.00

from the simulations. From this approach, we predicted an unbinding force of 60 ± 30 pN for the millisecond time scale. We expect experimental AFM data on this system to be available soon.

In this paper we focus on the microscopic interpretation of the unbinding forces of the ANO2/DNP-hapten complex in terms of physical interactions and unbinding pathways. To that end, we consider both the interactions between the ligand and individual ANO2 binding pocket residues and more structural aspects of the unbinding pathways. In particular, we focus on a possible structural heterogeneity of the unbinding pathway, which is assumed to cause significant scatter of unbinding forces. Such scatter has already been observed in a number of systems (Florin et al., 1994; Moy et al., 1994; Grubmüller et al., 1996), but was generally attributed to experimental or statistical error rather than structural heterogeneity. For the bound ANO2 complex, structural heterogeneity has been observed by NMR (Therriault et al., 1991; Martinez-Yamout and McConnell, 1994). Particularly, the light chain Tyr-31 was suggested to be rather flexible in these studies, and to contribute to induced fit motions upon binding (McConnell and Martinez-Yamout, 1996).

To investigate the microscopic nature of such structural heterogeneity and to assess its relevance for a proper description of the kinetics of binding and unbinding, we shall attempt to quantify the entropic contribution to the free energy barrier of enforced unbinding that results from that heterogeneity. To this end, principal component analyses of the unbinding trajectories will be used.

The importance of individual residues with respect to ligand binding is traditionally judged from site-directed mutagenesis of putative residues by measuring the change in free energy with respect to the wild type. Typically, that change can also be estimated from the x-ray structure by counting hydrogen bonds, salt bridges, or van der Waals contacts between ligand and binding pocket. Aiming at extending this procedure toward forces, we identified critical hydrogen bonds that are expected to significantly reduce the ANO2/DNP-hapten binding free energy.

To answer the question of how those crucial residues also affect unbinding forces, we modeled two mutants of ANO2 and carried out another series of FPMD simulations for each of the two mutants. In the first the mutant, the light chain Tyr-33 that interacts with the hapten molecule via a strong hydrogen bond was replaced by phenylalanine, which can not form such a hydrogen bond. The binding constant of that mutant is smaller than that of the wild type by a factor of 10 (Martinez-Yamout and McConnell, 1994). Accordingly, we also expected to find lower unbinding forces. In the other mutant, which has not been studied previously, the interaction between hapten and the binding pocket was increased by replacing Ile-96 by lysine. The lysine is expected to form an additional strong hydrogen bond to the hapten molecule,

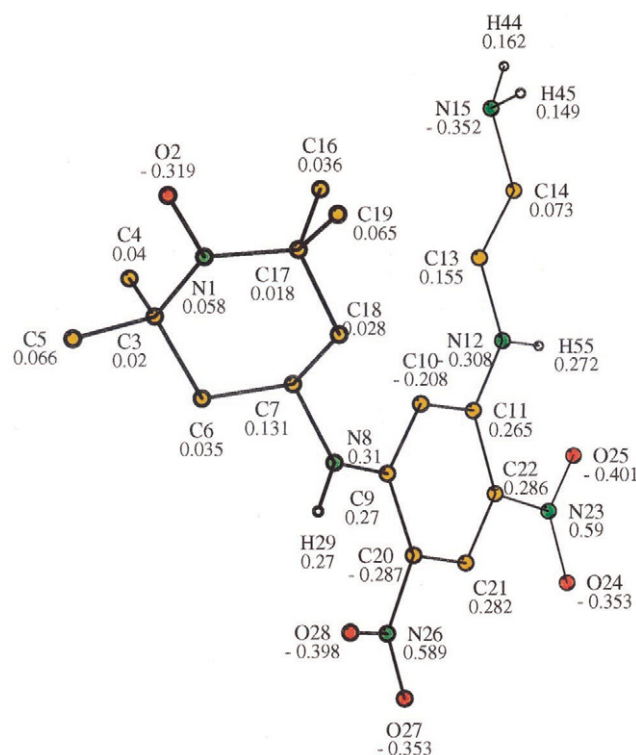


FIGURE 1 Structure of the spin-labeled dinitrophenyl hapten; shown are names and partial charges as computed with UNICHEM and used in the simulations.

which should give rise to an increased unbinding force for this mutant.

COMPUTATIONAL METHODS

Simulation systems and FPMD simulation methods

As a start, the x-ray structure of the ANO2 F_{ab} fragment complexed with the DNP-SL ligand (Brünger et al., 1991) was taken from the Brookhaven Protein Data Bank (Bernstein et al., 1977), entry 1baf. All molecular dynamics simulations were performed with the parallel MD program EGO (Eichinger et al., 2000) (Eichinger, M., H. Grubmüller, and H. Heller, 1995. User Manual for EGO_VIII, Release 2.0. Electronic access: www.mpibpc.gwdg.de/abteilungen/071/ego.html) and the CHARMM force field (Brooks et al., 1983). EGO allows efficient computation of Coulomb forces using the "fast multiple time step structure adapted multipole method" (Eichinger et al., 1997; Grubmüller and Tavan, 1998), so that no artificial truncation of these forces had to be applied (Brooks et al., 1983). For the DNP-hapten, partial charges were calculated with UNICHEM (Cray Research Inc. 1997. UniChem 3.0. 655 Lone Oak Drive, Eagan, MN 55151.) (see Fig. 1) using MNDO94, the AM1 Hamiltonian, ESP-fitting, and a dielectric constant of one. All force constants were taken from the CHARMM force field (Brooks et al., 1983). All simulations were carried out with an integration step size of 10^{-15} s. The length of chemical bonds involving hydrogen atoms was fixed (McCammon et al., 1977), and non-polar hydrogen atoms were treated through compound atoms (Brooks et al., 1983). No explicit term for the hydrogen bond energy was included within the force field.

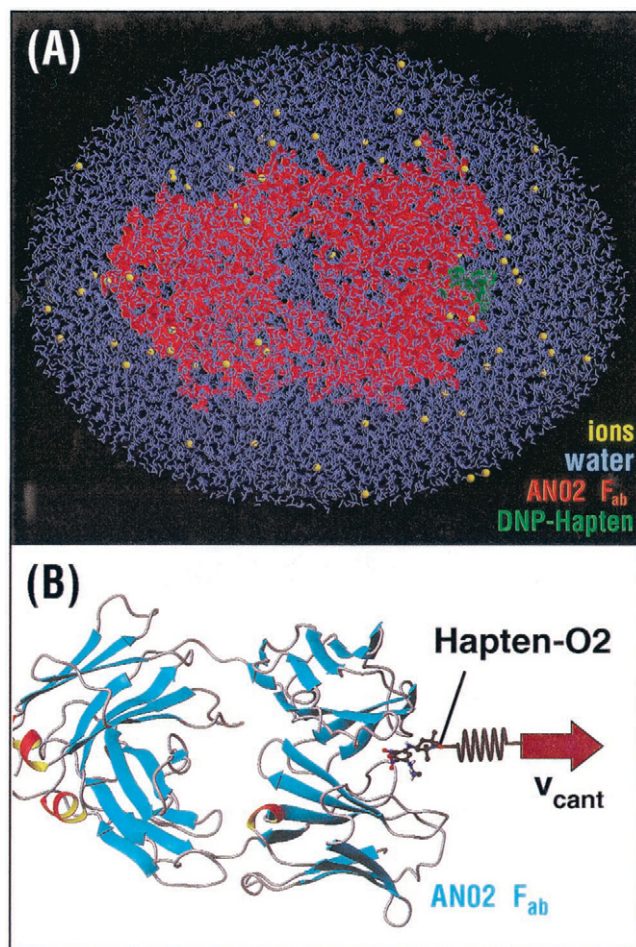


FIGURE 2 (A) Model of the solvated ANO2 (red)/DNP hapten (green) complex used in the molecular dynamics simulations described in the text. The complex has been surrounded by water molecules (blue); ions (yellow) were placed according to a Debye-Hückel distribution governed by the protein and hapten charges. (B) General setup of the force probe molecular dynamics (FPMD) simulations. Shown is the ANO2 F_{ab} fragment (ribbon plot) and the hapten molecule (ball-and-stick model). The oxygen atom O2 was subjected to a harmonic potential (spring), which was moved in the pulling direction (arrow) with constant pulling velocity v_{cant} .

A model for the solvated protein-ligand complex was built by surrounding the x-ray structure with a droplet containing 13,461 TIP3 (Jorgensen et al., 1983) water molecules, 34 Na^+ ions, and 41 Cl^- ions at physiological concentration using the program SOLVATE (Grubmüller, H. 1996. Solvate: a program to create atomic solvent models. Electronic access: www.mpibpc.gwdg.de/abteilungen/071/hgrub/solvate/docu.html) [see Fig. 2 A]. The ions were placed according to a Debye-Hückel distribution governed by the protein and hapten charges. The excess of seven Cl^- ions served to compensate the net positive charge of the complex. To keep the number of solvent molecules in the system as small as possible, a non-spherical solvent volume was chosen. The solvent surface was defined such that the minimum distance between the protein surface and the solvent surface was 20 Å near the binding pocket region and 12 Å elsewhere. The obtained simulation system comprised a total of 44,571 atoms.

To counterbalance surface tension and to prevent evaporation of water molecules, all surface water molecules were subjected to a “deformable boundary” (Brooks and Karplus, 1983), which has been adapted to water solvent and approximated by a quartic polynomial (Kossmann, 1997).

Additionally, all water molecules at the droplet surface were coupled to a heat bath of 300 K through stochastic forces obeying the fluctuation-dissipation theorem (Reif, 1965). A coupling constant of $\beta = 10 \text{ ps}^{-1}$ was used. All other atoms were weakly coupled to a heat bath ($\beta = 1 \text{ ps}^{-1}$) via velocity rescaling (Berendsen et al., 1984).

After energy-minimizing the whole system by 1000 steepest descent steps, the system was equilibrated for 1500 ps at 300 K. During equilibration, the stability of the complex was monitored via its root mean square (rms) deviation from the x-ray structure (“forward deviation”) and, as suggested by Stella and Melchionna (1998), also from the structure after equilibration (“backward deviation”). Following the suggestion of one of the referees, structural motions observed during equilibration were compared to structural flexibility obtained from a comparison of six related x-ray structures with each other using the program DynDom (Hayward and Berendsen, 1998).

For the rms computations four sets of heavy atoms were considered, namely those 1) of the complete protein-ligand complex, 2) of the variable, and 3) of the constant domain regions, and 4) of the binding pocket, respectively. Here, the binding pocket (referred to as “B” below) was defined as those residues that interact with the hapten molecule during the unbinding process, together with those parts of the hypervariable loops that are located close to the hapten molecule. These comprised residues 30–35(L), 47–52(L), and 86–99(L), as well as residues 30–36(H), 48–55(H), and 97–105(H), respectively. Here, and also in the following, (L) and (H) refer to the light and heavy chain.

The subsequent FPMD simulations were carried out as sketched in Fig. 2 B: in close resemblance to the pulling forces exerted in the single-molecule AFM experiment by the cantilever, the spin-labeled oxygen atom O2 of the hapten was subjected to a “spring potential” V_{spring} ,

$$V_{spring}(z_{O2}) := \frac{1}{2} k_{cant} [z_{O2}(t) - z_{cant}(t)]^2, \quad (1)$$

acting in a pulling direction on the z-coordinate z_{O2} of atom O2. Here, $z_{cant}(t)$ is the cantilever position. A spring constant of $k_{cant} = 280 \text{ pN/Å}$ was used throughout all simulations.

In the figure, V_{spring} is symbolized by a spring. Note that V_{spring} as defined above does not restrain sideward motions of the O2 atom, i.e., perpendicular to the z-direction, because such motions are also essentially unconstrained in the experiments. At the beginning of each FPMD simulation, the minimum position, $z_{cant}(0)$, of V_{spring} was placed at the position of atom O2, $z_{O2}(0)$. In the course of each simulation, V_{spring} was moved in the pulling direction with a constant pulling velocity v_{cant} , i.e., $z_{cant}(t) = z_{cant}(0) + v_{cant}t$.

To avoid larger sideward drift of the hapten, atom O2 was additionally subjected to a weak harmonic potential (spring constant: 14 pN/Å) perpendicular to the pulling direction. Finally, the center of mass of the protein (with hapten excluded) was kept in place by a relatively stiff harmonic potential (force constant: 2800 pN/Å). This setup allowed the protein to adapt to the enforced hapten unbinding, e.g., by rotations or intramolecular conformational motions like induced fit motions, also in close resemblance to typical AFM experiments.

During enforced unbinding, the pulling force $F_{pull}(t) = k_{cant}[z_{cant}(t) - z_{O2}(t)]$ acting on the oxygen atom was calculated and recorded every 100 fs. Thus, a “force profile” for each FPMD simulation was obtained as a function of cantilever position $z_{cant}(t)$. An unbinding force was defined as the maximum of the respective force profile, and the position of the O2 atom at that maximum was recorded to obtain an “unbinding length” (Heymann and Grubmüller, 1999a). The relatively stiff spring constant of $k_{cant} = 280 \text{ pN/Å}$ for the spring potential was chosen to provide high spatial resolution of the force profile of $k_B T/k_{cant} \approx 0.5 \text{ Å}$ while allowing thermal fluctuations of about the same size (Heymann and Grubmüller, 2000). High-frequency fluctuations of atom O2, which were artificially caused by the harmonic spring potential, were filtered by properly smoothing the force profiles (Grubmüller et al., 1996).

To characterize the velocity dependence of the unbinding forces and to allow proper statistical analysis of the unbinding pathways, a total of 58

FPMD simulations were carried out. For computation of the unbinding force as a function of the pulling velocity, 29 simulations were used. For these simulations, pulling velocities in the range between 0.1 and 50 m/s were chosen requiring simulation lengths between 30 and 7000 ps to complete the unbinding process in each case (Heymann and Grubmüller, 1999a). To study the structural heterogeneity of the enforced unbinding pathways, 20 FPMD simulations of 300 ps length each were carried out with identical pulling velocity, $v_{\text{cant}} = 5$ m/s. These simulations differed in their initial conformations, which were picked randomly from the last 820 ps of the 1500-ps equilibration trajectory.

Based on the equilibrated wild-type structure (taken from the equilibration phase at 1300 ps), two mutants of the AN02/DNP-hapten complex were modeled. Here our goal was to identify two mutation sites with opposite effects: the first one should decrease, the second one should increase the unbinding force. To that end, we first selected a hydrogen bond between Tyr-33(L) and the DNP molecule which, as judged from our prior FPMD simulations, strongly contributed to the unbinding force. That bond was then removed by a Y33F(L) mutation. The second mutant, I96K(L), was obtained by identifying the oxygen atom O25 of the DNP ring as a putative hydrogen bond acceptor, and by changing a suitably located isoleucine residue to lysine as a hydrogen bond donor.

To generate a model for the Y33F(L) mutant, the Tyr-33(L) side-chain hydroxyl group was removed and the force field was changed accordingly using the XPLOR (Brünger, 1988) phenylalanine force field parameters. The system was subsequently equilibrated for 50 ps.

The I96K(L) mutation required particular attention because here a charged NH_3^+ group had to be inserted. This was achieved using the molecular editor of the software package Quanta (Molecular Simulations Inc., 1997). Care was taken that no overlap with neighbored amino acids occurred. To compensate the positive net charge of lysine, a nearby sodium ion was removed. The resulting structure was equilibrated for 100 ps.

Starting from the respective equilibrated structures, each of the mutants was subjected to 22 FPMD simulations to allow accurate comparison of unbinding forces between the mutants and the wild type. Pulling velocities from 50 m/s to 2 m/s were used.

Analysis of FPMD unbinding simulations

For each of the FPMD simulations, changes of the interaction network between the hapten molecule and the AN02 F_{ab} fragment during unbinding were recorded and characterized by computing selected observables as a function of the cantilever position z_{cant} . These were the total electrostatic (Coulomb) and van der Waals (Lennard Jones) interactions 1) between hapten and AN02 and 2) between hapten and selected individual residues of the AN02 binding pocket, and formation and rupture of 3) hydrogen bonds and 4) water bridges between hapten and the relevant AN02 binding pocket residues. As relevant binding pocket residues we selected those residues which, in the course of the FPMD simulations, show significant electrostatic or van der Waals interactions with the hapten. Those were Trp-90(L), Tyr-33(L), Tyr-31(L), Asp-49(L), Ile-96(L), Gln-88(L), Trp-100(H), Tyr-51(H), Pro-101(H), and Tyr-54(H), and will be referred to as "R" below.

From the FPMD trajectories the electrostatic and van der Waals energies, respectively, among all atoms of the DNP molecule and all atoms of the protein and among all atoms of the DNP molecule and all atoms of the selected binding pocket residues were computed using XPLOR (Brünger, 1988). A cutoff of 10 Å was used for these energy computations. Energies were computed once per picosecond by averaging the values of 10 snapshots taken every 100 fs for each picosecond. To assess the integrity of the binding pocket during equilibration, this analysis has also been carried out on the 1500-ps equilibration trajectory for comparison.

Strength, formation, and rupture of hydrogen bonds between hapten and the binding pocket residues in the course of the unbinding process was monitored using a combined geometric and energetic criterion for the identification and quantification of hydrogen bonds (Kitao et al., 1993).

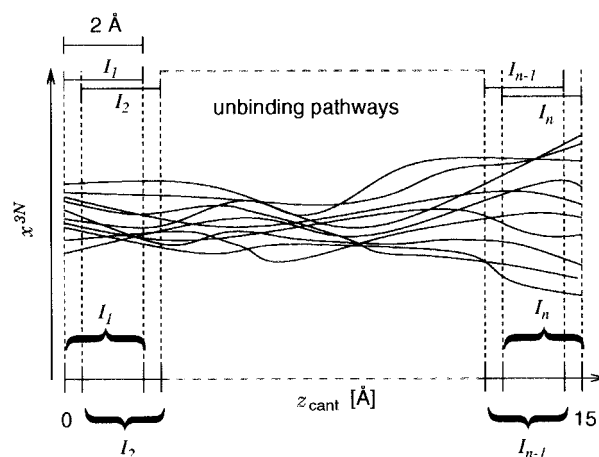


FIGURE 3 Sketch of the unbinding pathways of the hapten molecule out of the AN02 binding pocket. The volume covered by all unbinding pathways in a given interval I_i of cantilever positions z_{cant} is used to estimate the entropy of the complex.

Accordingly, a hydrogen bond was identified if the involved heavy atoms were closer to each other than 4 Å and if the sum of van der Waals and electrostatic energy was negative and its absolute value >1 kcal/mol. This sum was used to measure the strength of the identified hydrogen bonds. Water bridges between the hapten molecule and binding pocket residues were identified by requiring a water molecule to simultaneously form two hydrogen bonds, one to the hapten molecule and one to a binding pocket residue.

To structurally characterize the unbinding pathway of the hapten molecule and induced-fit motions of the whole binding pocket "B," FPMD trajectories were analyzed in detail. Particular attention was paid to ligand motions relative to the light chain residues and to the heavy chain residues of the binding pocket (cf. Fig. 13). Only trajectories from FPMD simulations with pulling velocities ($v_{\text{cant}} \leq 2$ m/s) were considered for this purpose because those frictional effects have been shown to be negligible. These simulations are thus assumed to best describe enforced unbinding as seen in the AFM experiments. Figures were prepared with Molscript (Kraulis, 1991) and MOLMOL (Koradi et al., 1996).

Principal component analysis (PCA) (Mardia et al., 1979) was used to estimate the size of the region in configurational space (of both ligand and binding pocket residues "B") covered by the ensemble of unbinding pathways obtained in our FPMD simulations. Generalizing the entropy estimate of protein structure ensembles suggested by Karplus and Kushick (1981) and improved by Schlitter (1993) to ensembles of trajectories, the PCA results were used to estimate the entropic contribution to the free energy along the unbinding pathway and, in particular, to the free energy barrier that governs the AN02/DNP-hapten binding kinetics. This procedure is described in the subsequent Theory section.

A total of 20 FPMD simulations has been used for the entropy estimate, each of 300 ps length. From each trajectory, 3000 coordinate sets (one per 100 fs) were taken for the PCA. These sets included the whole binding pocket "B" and the hapten molecule, comprising a total of 475 atoms.

As illustrated in Fig. 3 and explained in the Theory section, the coordinate sets were split into $n = 131$ overlapping subsets according to the reaction coordinate $z_{\text{cant}}(t)$ using intervals $I_i (i = 1, \dots, n)$ of 2 Å width each. The intervals were shifted along $z_{\text{cant}}(t)$ in 0.1 Å steps in the range between 0 Å (bound state) and 15 Å (unbound state). The obtained 131 coordinate subsets of 400 coordinate sets each were then evaluated using Eq. 11.

The relative contribution of the individual degrees of freedom to the configurational entropy change was calculated from the partial entropy

differences $\Delta S_m(z_{\text{cant}})$ with $m = 50, 55, 60, \dots, 100$. Larger values for m were not considered because at the chosen spatial resolution of $v_{\text{cant}}\Delta t = 2$ Å only 400 coordinate sets were available for each z_{cant} value.

THEORY: ENTROPY ESTIMATE FOR REACTION PATHWAYS

We assume a given ensemble $\{\mathbf{x}^{(i)}(t)\}_{i=1\dots n}$ of n MD trajectories along a reaction pathway with a Boltzmann ensemble $\{\mathbf{x}^{(i)}(0)\}_{i=1\dots n}$ of initial conditions (see Fig. 3). Here, $\mathbf{x}^{(i)}(t) \in \mathcal{R}^{3N}$ is the configuration vector of trajectory i at time t , where N is the number of atoms considered. Using this ensemble of trajectories, and generalizing the usual expression for the entropy in the canonical ensemble (Reif, 1965), we want to estimate how the entropy of this system changes in time as the system is forced to move along a reaction pathway,

$$S(t) = -k_B \int d^{3N} \mathbf{x} \rho(\mathbf{x}, t) \ln \rho(\mathbf{x}, t), \quad (2)$$

where $\rho(\mathbf{x}, t)$ is the time-dependent configuration space density that generates the trajectory ensemble $\{\mathbf{x}^{(i)}(t)\}$. In the above equation, the integral is taken over the full configurational space. (Because velocity-dependent forces are absent, the contribution of the momenta to the free energy is a constant and is thus irrelevant for the present purpose.)

Note that for the case at hand the ensemble moves along the unbinding reaction pathway with constant velocity, $z_{\text{cant}} = tv_{\text{cant}}$, hence $S(t)$ will be interpreted as the (configurational) entropy contribution to the free energy landscape along the unbinding reaction pathway as defined by the reaction coordinate z_{cant} . Note also that, in defining $S(t)$ via Eq. 2, we assume that all degrees of freedom perpendicular to the reaction pathway are in equilibrium at all times; the same assumption is made in Kramers' transition state theory (Eyring, 1935; Kramers, 1940).

For the stationary case, entropy estimates are available. As implicitly assumed by Karplus and Kushick (1981), $\rho(\mathbf{x})$ can be approximated by a multivariate Gaussian function $\tilde{\rho}(\mathbf{x})$ centered at \mathbf{x}_0 (Grubmüller, 1995),

$$\rho(\mathbf{x}) \approx \tilde{\rho}(\mathbf{x}) := \tilde{Z}^{-1} \exp \left[-\frac{1}{2} (\mathbf{x} - \mathbf{x}_0)^T \mathbf{A} (\mathbf{x} - \mathbf{x}_0) \right], \quad (3)$$

with partition function

$$\tilde{Z} := \int d^{3N} \mathbf{x} \exp \left[-\frac{1}{2} (\mathbf{x} - \mathbf{x}_0)^T \mathbf{A} (\mathbf{x} - \mathbf{x}_0) \right]. \quad (4)$$

Here, $\mathbf{A} \in \mathcal{R}^{3N \times 3N}$ is a symmetric, positive semidefinite matrix which defines the shape of the Gaussian. It is derived

from the covariance matrix of the coordinate sets (Gardiner, 1985), \mathbf{C} ,

$$\mathbf{A}^{-1} = \mathbf{C} := \langle [\mathbf{x}^{(i)} - \mathbf{x}_0][\mathbf{x}^{(i)} - \mathbf{x}_0]^T \rangle_i \quad \text{with} \quad \mathbf{x}_0 := \langle \mathbf{x}^{(i)} \rangle_i, \quad (5)$$

and can therefore be computed from an MD trajectory.

Within this approximation the (classical) entropy $S = -k_B \int d^{3N} \mathbf{x} \rho(\mathbf{x}) \ln \rho(\mathbf{x})$ can be computed (up to an additive constant) from the determinant of the covariance matrix (Karplus and Kushick, 1981), $S = \frac{1}{2} k_B \ln |\mathbf{C}|$, or, equivalently, from the product of the (nonzero) eigenvalues of the covariance matrix.

That estimate, however, suffers from instabilities caused by small eigenvalues that are unphysical in that these instabilities would vanish in a quantum-mechanical treatment of the above approximation. A correction has therefore been proposed (Schlitter, 1993),

$$S = \frac{1}{2} k_B \ln \left| \mathbf{C} + \mathbf{M}^{-1} \frac{\hbar^2}{k_B T e^2} \right|, \quad (6)$$

which provides a better entropy estimate, and also cures the instabilities. Here, \mathbf{M} is the diagonal mass matrix that contains the atomic masses, \hbar is Planck's constant, and $e = 2.718 \dots$ is the Euler number.

We shall use Eq. 6 to estimate the time-dependent entropy $S(t)$ defined in Eq. 2. However, a straightforward generalization of Eq. 6 is hampered by the fact that, because of the small number of trajectories usually available ($n = 20$ in our case) for each instance in time t_j , the covariance matrix computed from $\{\mathbf{x}^{(i)}(t_j)\}$ would be inaccurate due to statistical error. Furthermore, the covariance matrix would have too few ($n - 1$) nonvanishing eigenvalues, which means that only $n - 1$ out of the total number of $3N - 6$ internal degrees of freedom would be considered for the entropy estimate—most likely too few.

We therefore rewrite Eq. 2 as

$$S(t) = - \int dt' \int d^{3N} \mathbf{x} \rho(\mathbf{x}, t') \ln \rho(\mathbf{x}, t') \delta(t' - t), \quad (7)$$

where $\delta(t)$ is the Dirac delta function. Assuming that the inner integral in Eq. 7 is a smooth function on a short time scale Δt , $\delta(t)$ can be replaced by a (finite) square function, and an approximation for the entropy is obtained

$$S(t) \approx - \int dt' \int d^{3N} \mathbf{x} \rho(\mathbf{x}, t') \ln \rho(\mathbf{x}, t') \times \frac{1}{\Delta \pm} [\Theta(t) - \Theta(t + \Delta t)]. \quad (8)$$

Here $\Theta(t)$ is the step function, which is 0 for $t \leq 0$ and 1 otherwise. With the above condition of smoothness, $S(t)$ can

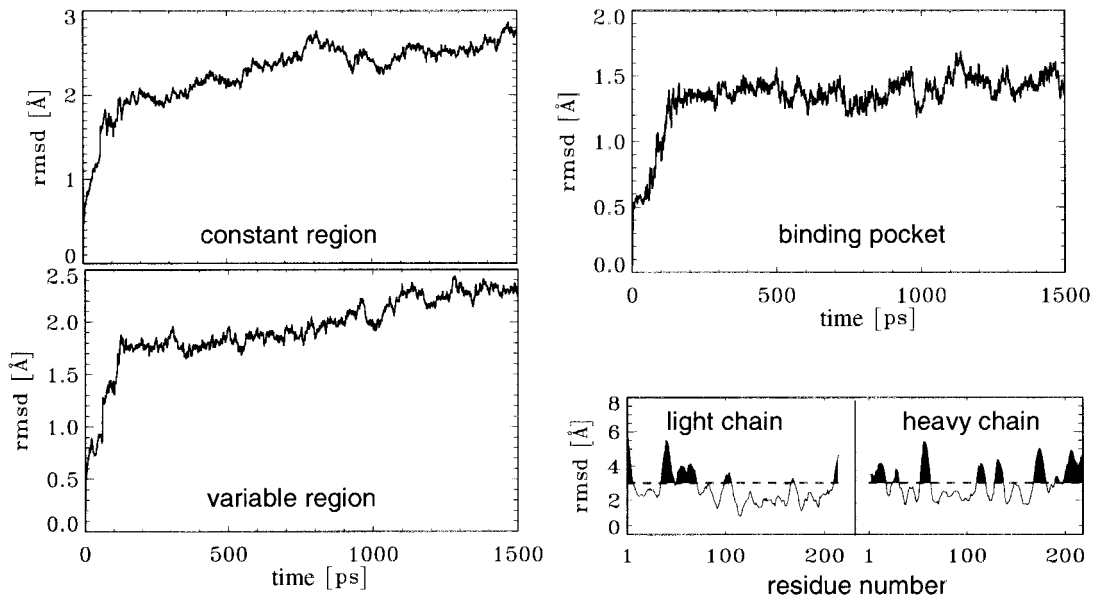


FIGURE 4 Root-mean-square (rms) deviation of selected regions of the AN02 antibody with respect to the x-ray structure during equilibration. Considered are the constant region (*top left*), the variable region (*bottom left*), and the binding pocket region (*top right*), respectively. Root-mean-square deviations per residue are shown in the bottom right panel where rms deviations of >3 Å are highlighted in black.

further be approximated by the time-averaged value of the inner integral,

$$S(t) \approx - \int d^3N \mathbf{x} \langle \rho(\mathbf{x}, t') \ln \rho(\mathbf{x}, t') \rangle_{t'=t \dots t+\Delta t},$$

$$\approx - \int d^3N \mathbf{x} \langle \rho(\mathbf{x}, t') \rangle_{t'=t \dots t+\Delta t} \ln \langle \rho(\mathbf{x}, t') \rangle_{t'=t \dots t+\Delta t},$$

(9)

for which Eq. 6 is applicable with the understanding that now the *subensemble* of structures $\{\mathbf{x}^{(i)}(t_j)\}_{t \leq t_j < t+\Delta t}$ is to be used for the computation of the covariance matrix \mathbf{C} , which thus becomes a function of t . For sufficiently large Δt , that ensemble is large enough such that a sufficient number of degrees of freedom enters into the entropy estimate.

Using the subensemble of the first interval as the (arbitrarily chosen) zero point, the entropy change along the unbinding reaction pathway is then readily estimated,

$$\Delta S(z_{\text{cant}}) = \Delta S(tv_{\text{cant}})$$

$$= \frac{1}{2} k_B \ln \frac{|\mathbf{C}(t) + \mathbf{M}^{-1} \hbar^2 / (k_B T e^2)|}{|\mathbf{C}(0) + \mathbf{M}^{-1} \hbar^2 / (k_B T e^2)|}. \quad (10)$$

The resulting entropy difference $\Delta S(z_{\text{cant}})$ serves to quantify the entropic contribution to the free energy caused by the structural heterogeneity of the unbinding pathways. Furthermore, by replacing the two determinants in Eq. 10 by

products of the respective eigenvalues $\lambda_l(t)$ (which we assume for each t to be ordered by decreasing size),

$$\Delta S(z_{\text{cant}}) = \frac{1}{2} k_B \sum_{l=1}^{3N} \ln \frac{\lambda_l(t)}{\lambda_l(0)}, \quad (11)$$

the relative contribution of each (collective) degree of freedom l to the entropy change $\Delta S(z_{\text{cant}})$ can readily be seen. Because, typically, this relative contribution is large for those degrees of freedom with large eigenvalues (García, 1992; Kitao et al., 1991; Amadei et al., 1993; Schulze et al., 2000) and vanishes for those with small eigenvalues, partial entropies $\Delta S_m(z_{\text{cant}})$ of the first m terms in Eq. 11 can be used as a check for proper convergence.

RESULTS AND DISCUSSION

Equilibration

Fig. 4 shows the rms deviation for selected regions of the AN02 antibody during equilibration. From the traces for the constant region (*top left*), the variable region (*bottom left*), and the binding pocket region “B” (*top right*), a significant increase from the x-ray structure ($t = 0$) during the first 100 ps of the equilibration is seen. After this short relaxation period, the region of interest, namely the binding pocket region, shows no further drift from the x-ray structure and stabilizes at the relatively small rms value of 1.4 Å. Small drifts are seen, however, for the constant and variable regions, respectively.

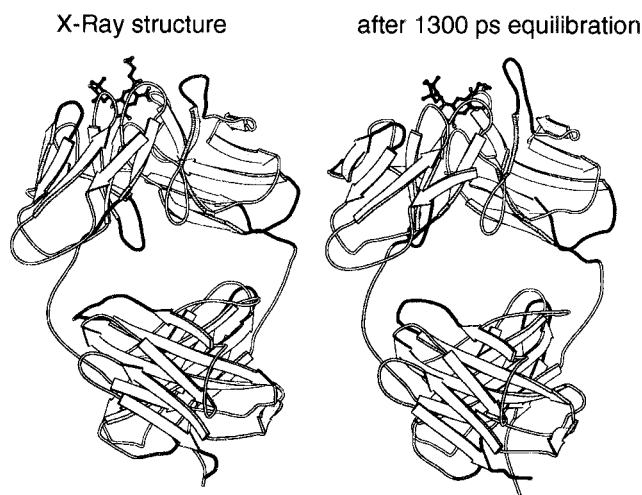


FIGURE 5 Comparison of the AN02/DNP-hapten x-ray structure (*left*) with a representative snapshot after equilibration (*right*). Regions with an rms deviation >3 Å are shown in black (cf. Fig. 4, *bottom right*).

Although the stability of the binding pocket region seems to be established, the slow rms drifts of the constant and the variable regions deserved further study. To that end, Fig. 4 (*bottom right*) plots the rms deviation per residue; rms deviations of 3 Å are highlighted in black. These regions of high mobility are also highlighted in black in Fig. 5, where the AN02 x-ray structure (*left*) and the structure after equilibration (*right*) are shown as ribbon plots. As can be seen, all high-mobility regions are loops at the protein surface. In contrast, the β scaffold, and in particular the binding pocket, appear nearly unchanged.

An even larger rms drift shows up in Fig. 6, where the rms deviation of the complete AN02/hapten complex during equilibration is shown (*heavy line*). Here an rms value of 3.1 Å is reached at the end of the equilibration phase, and no clear evidence for convergence is seen. That deviation is significantly larger than that of the individual chains, as seen in Fig. 4 (*left*), which suggests that this increased

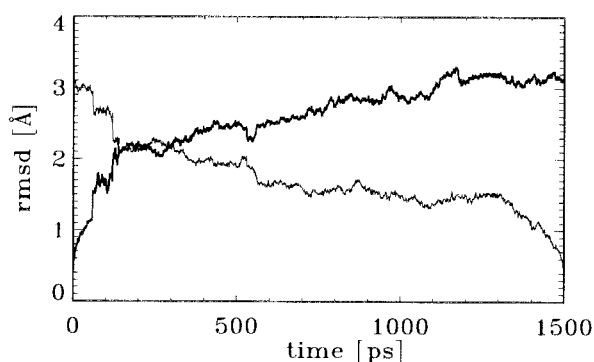


FIGURE 6 Root-mean-square (rms) deviation of the AN02/DNP-hapten complex from the x-ray structure ("forward deviation," *heavy line*) and from the final, equilibrated structure ("backward deviation," *thin line*).

deviation is mainly due to very slow motions of the constant region relative to the variable region.

In this case, the relatively large drift of 3.1 Å seen for the whole F_{ab} fragment would likely result from (equilibrium) sampling motions of the domains rather than from (non-equilibrium) relaxation motions. To distinguish between these two cases, it has been suggested (Stella and Melchionna, 1998) to additionally consider the *backward* deviation (*thin line* in Fig. 6), which measures the deviation from the equilibrated (final) structure.

In contrast to the forward rms deviation, the backward deviation stays small (below 1.7 Å) between 550 and 1300 ps, and exhibits only slight drift during that period. Note also that the abrupt drop to zero between 1300 and 1500 ps must be attributed to equilibrium fluctuations, because otherwise a corresponding rms change would show up during that period in the forward deviation as well, which is not the case. Therefore, following the argumentation of Stella and Melchionna (1998), we assume that the main relaxation motions take place during the first 550 ps of the equilibration phase and that the period after 550 ps, in particular the obvious rms drift, is characterized by slow equilibrium sampling motions.

Closer inspection of snapshots during equilibration (not shown) supports this view and reveals a hinge bending motion of the variable region domain of the F_{ab} fragment with respect to the constant region domain around the two loops connecting these two regions. The variable region, which contains the binding pocket, stayed unchanged during equilibration.

This observation is in full agreement with the conformational flexibility of the F_{ab} fragment as obtained from a selection of AN02 homologs (Brookhaven Protein Data Bank entries 1hin:L, 1lhf:L, 1him:J, 1him:H, 1hil:C, and 1hil:A), which have been identified as "structural neighbors" with SCOP (Murzin et al., 1995). From these structures, and in a similar manner as suggested previously (Van Aalten et al., 1997), a hinge-bending flexibility between the constant and variable domain region was identified with angles between 7 and 16° and a hinge axis similar to the one observed in the MD simulation (data not shown). Averaged over all 15 pairs of the above six structures, the heavy atom mean rms deviation is 1.33 Å for the whole F_{ab} fragment and 0.98 Å and 1.08 Å for the variable and constant domains, respectively, which also documents the significant contribution of the interdomain flexibility to the overall rms deviations.

The interaction network that stabilizes the hapten molecule within the binding pocket has been characterized from the x-ray structure and other studies (Brünger et al., 1991; Anglister et al., 1987; Leahy et al., 1988; Theriault et al., 1991, 1993; Martinez-Yamout and McConnell, 1994). These interactions, shown in Fig. 7, are unchanged after the equilibration phase. The DNP ring of the hapten molecule (*gray*) is buried in a tryptophane sandwich formed by Trp-

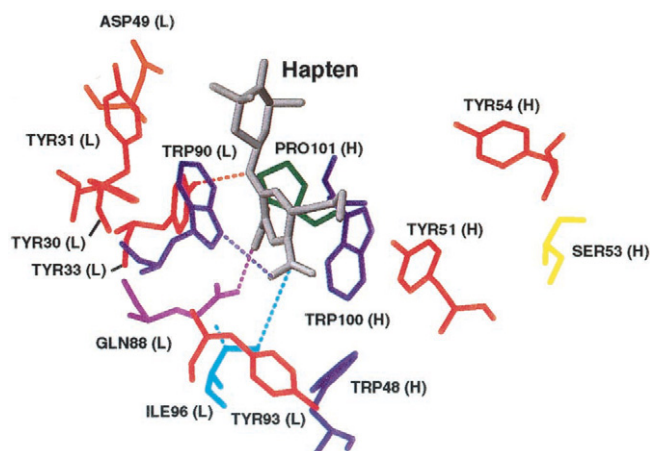


FIGURE 7 Interaction network between bound DNP-hapten (gray) and AN02 binding pocket after equilibration. Strong hydrogen bonds between the hapten and binding pocket residues are indicated by dotted lines. Residues are numbered as in the x-ray structure (Brünger et al., 1991) and differ by one from the numbering used by Martinez-Yamout and McConnell (1994).

90(L) and Trp-100(H), and stabilized by contacts between the aromatic rings. Several hydrogen bonds further stabilize the complex; the strongest are shown in the figure (*dashed lines*). Here, the hydrogen bond between Tyr-33(L) and an amino group (N8,H29; cf. Fig. 1) at the linkage of the two hapten rings is the most stable. Also observed are hydrogen bonds to Trp-90(L), Gln-88(L), and Ile-96(L), as well as (not shown) a weak one to Tyr-31(L) and a fluctuating one to Asp-49(L).

Fig. 8 quantifies the above statement. Shown is the strength of the relevant hydrogen bonds and that of the van der Waals contacts between hapten and the relevant binding pocket residues “R” (encoded via the thickness of the lines) during the equilibration period. Although the strength of the interactions fluctuates, as can be expected from the dynamics of the system, no overall and significant change of the

interaction “fingerprint” is observed. Consider, e.g., the hydrogen bond to Tyr-33(L), which weakens at 970 ps, but is completely restored afterward at 1150 ps. With a possible exception of the bond to Asp-49(L), which appears somewhat weaker than in the x-ray structure, the interaction network and, thus, the binding pocket region remain intact after equilibration.

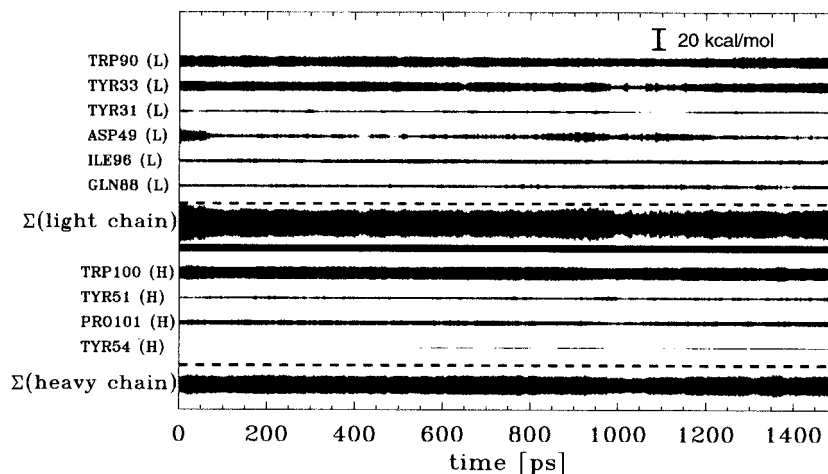
From the above results we conclude that the AN02/hapten bond is described by our simulations to sufficient accuracy. Thus the obtained equilibrated structure provides an appropriate starting point for the subsequent FPMD simulations, the results of which will be described. We also consider the period between 550 and 1500 ps suitable to provide an ensemble from which independent starting structures for otherwise identical FPMD simulations can be extracted as a check for reproducibility and to improve the statistics of the simulation results.

Enforced unbinding of the AN02 antibody/hapten complex

Two sets of FPMD simulations were carried out. To study the variation of unbinding force on the pulling velocity v_{cant} and to check to what extent unbinding pathways and force profiles depend on v_{cant} , 29 simulations with v_{cant} between 0.1 and 50 m/s were carried out. For structural analysis and computation of force profiles, only the simulations with $v_{\text{cant}} < 2$ m/s were considered, for which friction was found to be negligible (Heymann and Grubmüller, 1999a). Within that range, as already described (Heymann and Grubmüller, 1999a), unbinding forces were found to agree well with the expected logarithmic velocity dependency (Bell, 1978; Grubmüller et al., 1996; Evans and Ritchie, 1997; Israilewitz et al., 1997).

To study the nature and extent of structural heterogeneity of the unbinding pathway, an additional 20 FPMD simulations were carried out and analyzed, each of 300 ps length.

FIGURE 8 Sum of electrostatic and van der Waals interactions between DNP-hapten and individual residues of the light chain (*top half of the plot*) and the heavy chain (*bottom half*) during equilibration. The thickness of the lines reflects the strength of the interactions.



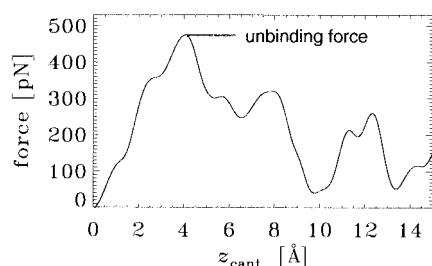


FIGURE 9 “Force profile” of enforced AN02/DNP-hapten unbinding. Shown is the pulling force exerted on the hapten molecule during unbinding as a function of cantilever position z_{cant} . The force maximum at $z_{\text{cant}} = 4.0$ Å is interpreted as the unbinding force.

These otherwise identical simulations differed in their initial conformations, which were randomly chosen from the last 820 ps of the equilibration phase.

Force profile

Fig. 9 shows a typical force profile, obtained at $v_{\text{cant}} = 1$ m/s. Like the one shown, all computed force profiles exhibit several force barriers in the course of the unbinding process. For most of them, the force maximum (which determines the unbinding force) is located at cantilever positions $z_{\text{cant}} \leq 4$ Å; i.e., the force maximum is traversed rather early in the unbinding process, and correspondingly short unbinding lengths were obtained. Furthermore, for $z_{\text{cant}} \leq 4$ Å all force profiles exhibit very similar shapes, whereas for $z_{\text{cant}} > 4$ Å, significant variations appear.

This finding suggests to split the unbinding pathway into two parts. The similar force profiles of the first 4 Å (subsequently denoted as part A) as obtained from several FPMD simulations indicate that the geometry and the sequence of hydrogen bond ruptures during unbinding should vary only slightly, which turned out to be the case. The following subsection characterizes this part of the unbinding pathway.

In contrast, the subsequent portion of the unbinding pathway (denoted as part B) exhibits a surprisingly large structural heterogeneity, which causes the observed variation of the respective parts of the force profiles (data not shown). This heterogeneity is one main focus of this paper and is analyzed in two further subsections.

Initial unbinding steps

Three snapshots at $z_{\text{cant}} = 0$ Å, 2 Å, and 4 Å, respectively (Fig. 10) illustrate the first unbinding steps of the AN02/DNP-hapten complex. Here the hydrogen bonds and van der Waals contacts are indicated by dashed lines. The first significant event in the unbinding process, seen in all FPMD simulations, is the breakage of the (relatively weak) hydrogen bond between the side-chain nitrogen atom of Gln-

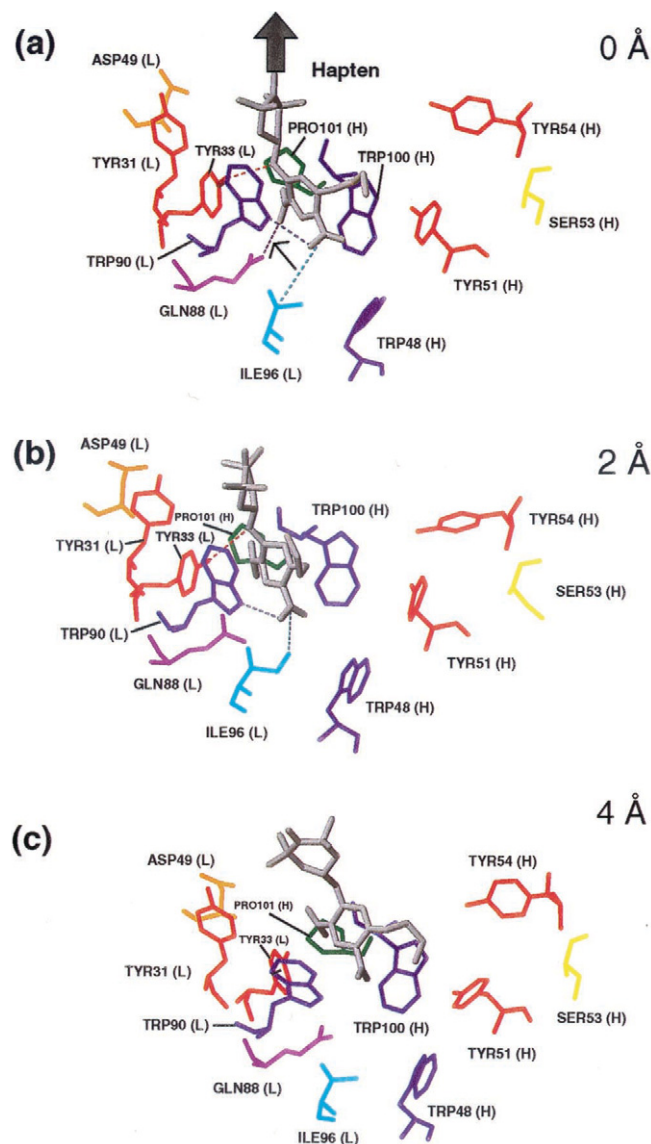


FIGURE 10 Three snapshots (a–c) of the initial steps (part A) of the hapten (gray) unbinding pathway. Shown are relevant residues of the binding pocket and the main interactions observed in the simulations such as hydrogen bond and van der Waals contacts (dashed lines). The respective cantilever positions z_{cant} are indicated at the right. The black arrow indicates the pulling direction.

88(L) and the nitro group (N26,O27,O28) of the hapten (small arrow in the first snapshot). Subsequently, and caused by this rupture, the hapten DNP ring rotates in a clockwise direction, and the nitro group is slightly reoriented toward the exit of the binding pocket. Simultaneously, a water bridge between Gln-88(L) and the same nitro group (not shown) disappears.

Subsequently (second and third snapshot), several changes in the interaction network between the hapten molecule and the binding pocket residues occur, apparently independently of each other. Accordingly, the exact se-

quence of these changes varies among the simulations and is therefore left undefined.

One of these is that van der Waals contacts between the Ile-96(L) side chain and the nitro group of the hapten DNP ring weaken, and the hydrogen bond between the nitrogen atom in the 5-ring of Trp-90(L) and the oxygen atom in the same hapten nitro group ruptures, as also does the hydrogen bond between the hydroxyl group of Tyr-33(L) and the amino group. The latter event induces a conformational change of the hapten during which the linkage between the two rings suddenly flips into another configuration, resulting in a slight motion of the hapten molecule away from the light chain and toward the heavy chain. In parallel, the side chains of Trp-90(L) and Trp-100(H) move away from the hapten DNP ring, thereby opening the sandwich configuration. Additionally, the Trp-100(H) side-chain moves deeper into the binding pocket, thereby showing considerable flexibility. The changed orientation of the Trp-100(H) side-chain causes, in turn, an increased flexibility of the amino-ethyl-amino chain of the hapten molecule. Several of the FPMD simulations show transient hydrogen bonds between this chain and the hydroxyl groups of Tyr-51(H) and Tyr-54(H).

All these events are accompanied by an initial unbinding motion of the hapten molecule, whose DNP ring moves out of the tryptophane sandwich toward the exit of the binding pocket.

Structural heterogeneity

The subsequent unbinding motions show much larger conformational variations. Interestingly, upon closer analysis, the *chronological order* of the previous steps described so far turned out to determine the nature of the subsequent unbinding motions. In particular, two critical events were identified that acts as a “switch” and thus completely determine the subsequent steps. These two critical events were 1) rupture of the hydrogen bond to Tyr-33(L), and 2) opening of the tryptophane sandwich and release of the hapten DNP ring.

Fig. 11 characterizes the two variants by two series of snapshots of the unbinding process, which we denote as “light chain route” (*left*) and “heavy chain route” (*right*), respectively. The snapshots were obtained from two simulations that both started from the same configuration (*top*). The simulations were selected because they show the features of both pathways particularly clearly. Other simulations, the complete ensemble of which will be analyzed further below, can be considered as mixtures of these two prototypic pathways, sharing features of both. These are typically those for which the two critical events overlap in time such that their chronological order is not well defined.

Those simulations in which the tryptophane sandwich opens early before rupture of the hydrogen bond between Tyr-33(L) and hapten proceed with the “light chain route.”

Here, after the DNP ring is released from the sandwich, the hapten molecule is free to move toward the light chain (first snapshot on the left). As a consequence, a number of transient and relatively strong interactions [mainly van der Waals contacts and hydrogens bonds (*dashed lines*) and water bridges (not shown)] form between the hapten molecule and several residues of the light chain, in particular to Asp-49(L) and Tyr-31(L) (second snapshot). No strong interactions to heavy chain residues are seen.

Those simulations in which the hydrogen bond between Tyr-33(L) and hapten ruptures earlier, i.e., while the tryptophane sandwich is still intact, proceed with the “heavy chain route” (snapshots on the right). Apparently, and although the hapten DNP ring is still stabilized by the tryptophane sandwich, rupture of this critical hydrogen bond induces a jump of the hapten amino group toward the heavy chain. The subsequent strong interactions between the amino-ethyl-amino chain of the hapten molecule and Tyr-51(H) and Tyr-54(H) (*middle*), as well as between the nitro group (N23,O24,O25) of the hapten DNP ring and the hydroxyl group of Tyr-54(H) (*bottom*) forces the hapten molecule to “slide” along the heavy chain side of the binding pocket. Here, no interactions with light chain residues are observed.

The top two panels of Fig. 12 serve to quantify and confirm the above qualitative picture of both the “light chain route” (*left panels*) and the “heavy chain route” (*right panels*). Shown are “interaction fingerprints” which display, encoded by the thickness of the respective traces, the strength of interactions between the hapten molecule and selected binding pocket residues in the course of the simulations and, via $z_{\text{cant}} = tv_{\text{cant}}$, as a function of cantilever position.

As can be seen, for the “light chain route” the interactions between the hapten molecule and the light chain residues persist much longer (until $z_{\text{cant}} \approx 10 \text{ \AA}$) than for the “heavy chain route” (until $z_{\text{cant}} \approx 5 \text{ \AA}$). This is observed for both the interactions to individual binding pocket residues and the total interaction energy between the hapten molecule and the light chain [$\Sigma(\text{lightchain})$] and the heavy chain [$\Sigma(\text{heavychain})$].

The opposite correlation, though somewhat weaker, is observed for the interactions to heavy chain residues. Although, in contrast to the interactions with the light chain residues, no significant difference in the *duration* of these interactions is seen, they become significantly weaker at $z_{\text{cant}} \approx 4 \text{ \AA}$ for the “light chain route” as compared to the “heavy chain route.” The critical interaction here is the hydrogen bond between the hapten molecule and Tyr-54(H), which is formed transiently in the range $z_{\text{cant}} = 4\text{--}8 \text{ \AA}$ for the “heavy chain route,” but which is nearly absent for the “light chain route.” There, also, the interactions to Tyr-54(L) vanish at an earlier stage of the unbinding process.

Also, the force profiles reflect which route is taken (*bottom panels* in Fig. 12). In particular, the unbinding force, i.e., the maximum of the force profile, correlates with the unbinding route: significantly larger unbinding forces (400–450 pN) are observed for the “heavy chain route” than for

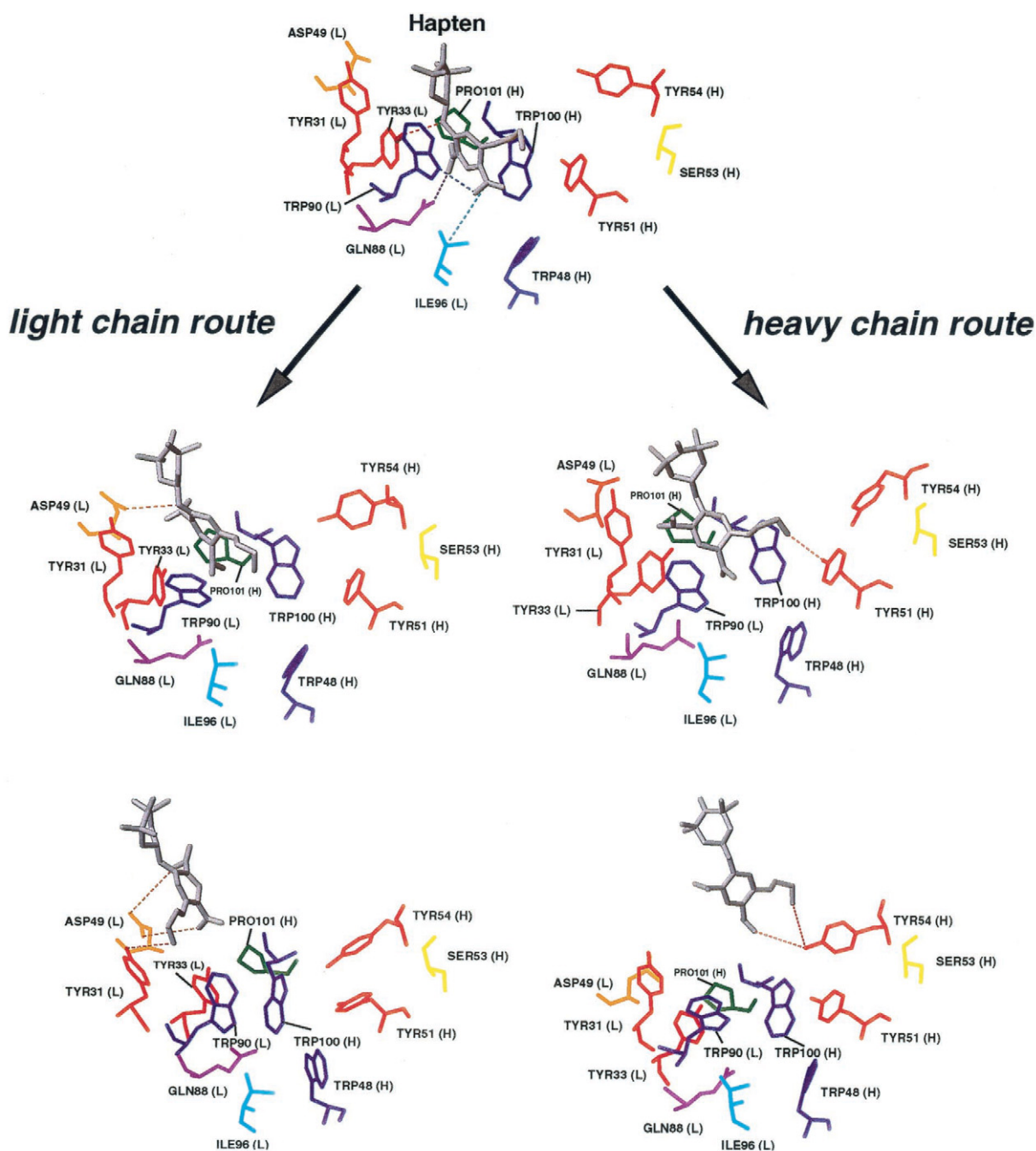


FIGURE 11 Snapshots taken from FPMD simulations with varying unbinding pathways. The left snapshots illustrate the “light chain route,” the right ones the “heavy chain route.” The cantilever positions of the snapshots are $z_{\text{cant}} \approx 0 \text{ \AA}$ (top), $z_{\text{cant}} \approx 5 \text{ \AA}$ (middle), $z_{\text{cant}} \approx 10 \text{ \AA}$ (bottom), respectively.

the “light chain route” (250–300 pN). This finding explains the surprisingly large scatter of unbinding forces (Heymann and Grubmüller, 1999a), which we found to be larger than, e.g., in the streptavidin/biotin system studied earlier (Grubmüller et al., 1996). Given the accuracy of single-molecule AFM experiments, we expect the scatter to also show up in such experiments, for example as a deviation from the usual Gaussian distribution of measured unbinding forces. In con-

trast, the unbinding length appears to be unaffected, as should also therefore be the case for the logarithmic slope of unbinding forces when measured as a function of loading rate.

We now consider the whole ensemble of the 20 FPMD simulations carried out at $v_{\text{cant}} = 5 \text{ m/s}$ as described in the Methods section. As stated above and easily discernible in Fig. 13, the 20 unbinding trajectories cover a whole spectrum of unbinding pathways in which the “light chain route”

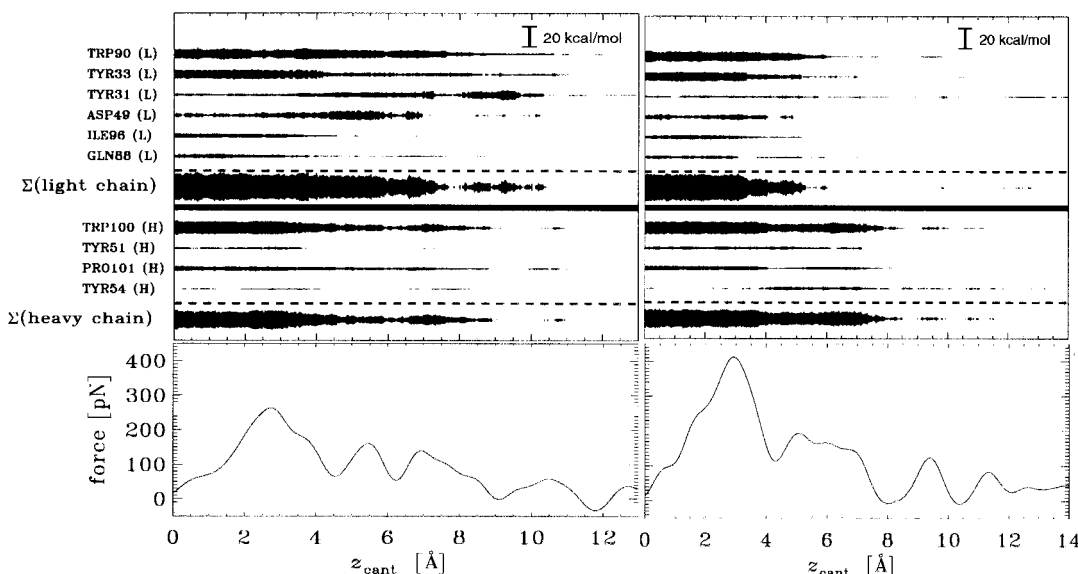


FIGURE 12 Interaction “fingerprints” (*top*) and force profiles (*bottom*) obtained from two representative simulations that took the “light chain route” (*left*) and the “heavy chain route” (*right*), respectively. The “fingerprints” show the strength of individual interactions between the hapten molecule and the relevant binding pocket residues “R” and the total interaction energies between the hapten molecule and the light chain [$\Sigma(\text{lightchain})$] and the heavy chain [$\Sigma(\text{heavychain})$], respectively, as a function of cantilever position z_{cant} . The thickness of the lines denotes the interaction energy.

and the “heavy chain route” appear as extreme cases. Shown are (in a different color for each of the 20 FPMD simulations) the traces of the hapten center of mass as it moves out of the binding pocket during unbinding. The initial (equilibrated) structure is shown in gray (hapten) and orange (binding pocket residues). Also shown are the unbound states for the “light chain route” as well as for the “heavy chain route,” with the final structures of the hapten shown in yellow and green, respectively.

As can be seen, for the initial phase of the simulations (part A), the traces stay within a relatively narrow region; after the force maximum at $z_{\text{cant}} \approx 4$ Å (start of part B, indicated by a red dashed line), the traces spread out like a fan. This transition point is defined by the release of the hapten DNP ring from the tryptophan sandwich and coincides with the force maximum. Such structural heterogeneity is a well-known feature of ensembles of protein *structures*, which was first observed by Frauenfelder and others (Ansari et al., 1985; Frauenfelder et al., 1989) and was later seen also in MD simulations (Elber and Karplus, 1987; Schulze et al., 2000). For the AN02/DNP system, our FPMD simulations predict a similar structural heterogeneity for (nonequilibrium) *reaction pathways*. Such structural heterogeneity should give rise to a significant entropic contribution to the free energy barrier that separates the bound from the unbound state. The following subsection attempts to estimate the size of that entropic contribution.

Entropic contribution to the AN02/DNP-hapten bond

As a measure for the entropic contribution to the free energy landscape along the unbinding pathway, we used the volume in

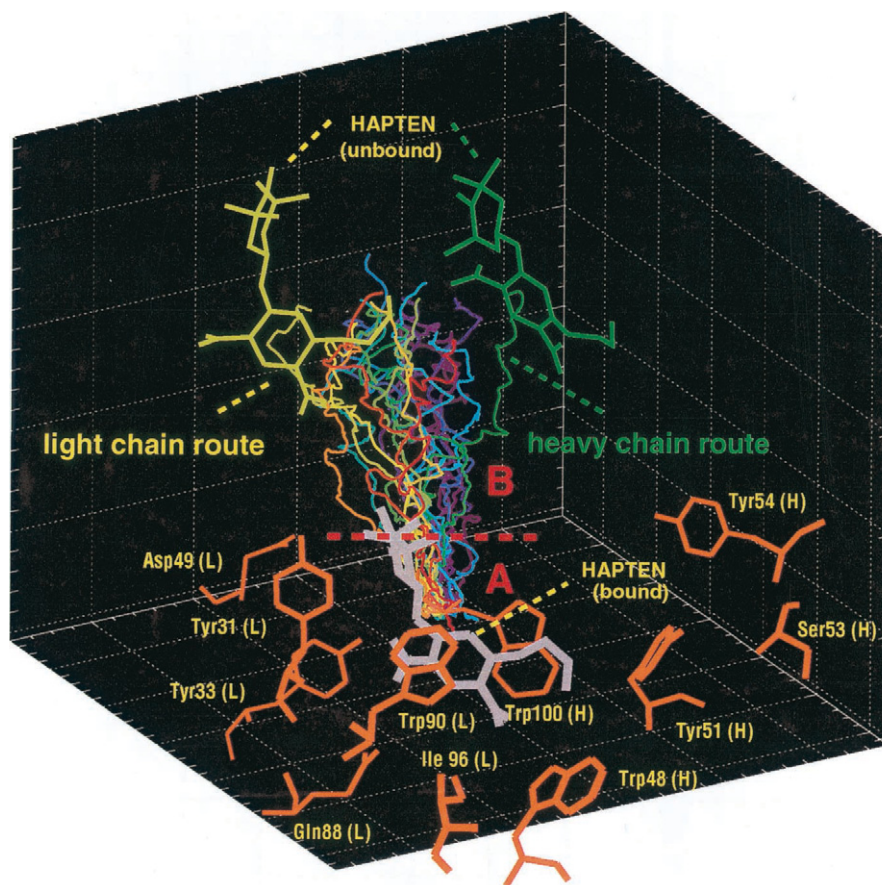
configurational space that is occupied by the pathway bundle obtained from the 20 FPMD simulations. The relative volume change as a function of z_{cant} (with respect to the bound state) has been estimated by PCA analysis (Eqs. 10 and 11).

Fig. 14 shows entropy estimates for $T = 300$ K, taking into account the $m = 50, 55, 60, \dots, 100$ most significant degrees of freedom, as defined by the eigenvalues of the covariance matrix. As can be seen, the curves converge well above $m = 70$, thereby also providing an estimate of the number of degrees of freedom that change their dynamics in the course of unbinding. The fact that the entropy estimate converges at a smaller number (70) of dimensions than the number of coordinate sets used for each value of z_{cant} (400) also justifies the choice of the size of the intervals I_i as defined in Fig. 3.

The obtained entropy landscape shows a rapid increase for part B of the unbinding pathway ($z_{\text{cant}} > 4$ Å), in agreement with the observation of a pronounced divergence of unbinding pathways after release of the hapten DNP ring from the tryptophan sandwich at that point. Given the total unbinding free energy of 15 kcal/mol, this entropy jump of ~ 6 kcal/mol is indeed a significant contribution.

A few caveats are, however, mandatory. First, nonequilibrium reaction pathways have been used. This generally underestimates the equilibrium values because the region of phase space that is sampled with the relatively short simulation time may be smaller than the region covered by an equilibrium Boltzmann ensemble. Second, our approach implies that all degrees of freedom perpendicular to the reaction pathway are in equilibrium at all times. This assumption is often made, e.g., in Kramers' transition state

FIGURE 13 Unbinding pathways for 20 FPMD simulations, each with pulling velocity 5 m/s, but slightly differing initial conditions. Shown are the traces (colored lines) of the hapten center of mass and the starting structure (hapten: gray; binding pocket residues: orange). For the two extreme routes, the unbound hapten molecule as seen at the end of the simulation at $z_{\text{cant}} = 15.0 \text{ \AA}$ is shown in yellow and green. The red dashed line indicates the force maximum that separates the unbinding pathway into the two parts A and B referred to in the text.



theory (Eyring, 1935; Kramers, 1940) or within the molecular dynamics field, for the calculation of free energies by “umbrella sampling” or related methods. The fact that the observed pathways overlap and that jumps between path-

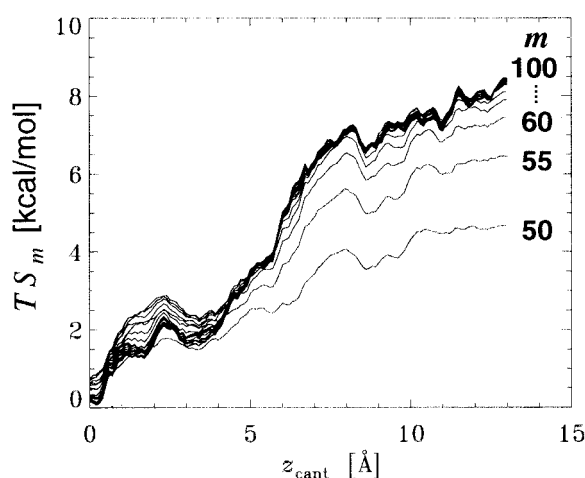


FIGURE 14 Entropic contribution $TS_m(z_{\text{cant}})$ (at $T = 300 \text{ K}$) to the free energy landscape along the unbinding reaction pathway as a function of cantilever position z_{cant} . The individual traces have been obtained by taking the $m = 50, 55, 60, \dots, 100$ most significant degrees of freedom into account.

ways are seen suggests that for AN02/DNP unbinding this assumption is not severely violated.

The third caveat concerns a more technical issue. Although generation of an ensemble of 20 trajectories is clearly an improvement with respect to the many studies that are based on one or two simulations, it is still a very small ensemble for the purpose of an entropy estimate. By trading off spatial resolution, we have increased that ensemble to 400 such that up to hundred collective degrees of freedom could be reasonably considered. Indeed, within this limited range, convergence is seen. However, by including adjacent coordinate sets taken from the same trajectory into our estimate, we have introduced correlations. Therefore, the *effective* ensemble size may be <400 , in which case the seen convergence might be artificial. We assume the effect of limited ensemble size to be more severe for phase B of the unbinding pathway, where a larger region of configuration space has been sampled, resulting in an underestimate of the corresponding entropic contribution as well.

Finally, to avoid that the hapten encounters the boundary region of the simulation system, we have slightly restricted the motion of the hapten by subjecting atom O2 to a weak harmonic potential perpendicular to the pulling direction. Accordingly, two of the three degrees of free-

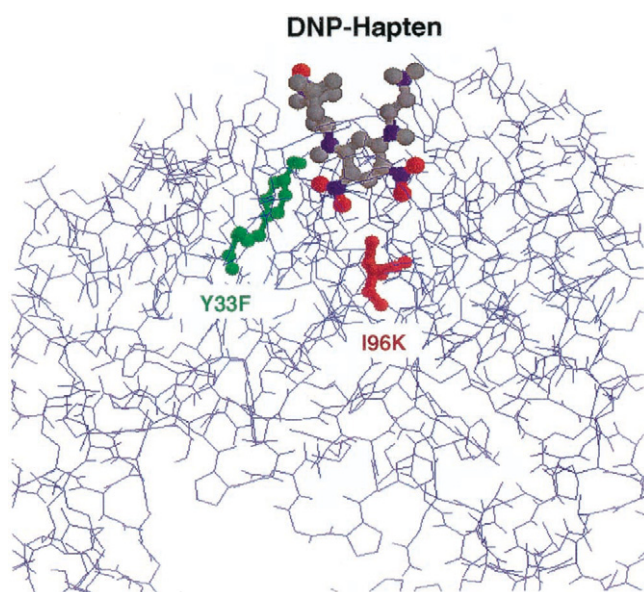


FIGURE 15 Location of the two site-directed light chain mutants of the ANO2/DNP-hapten complex, Y33F(L) (green) and I96K(L) (red), described in the text.

dom describing the center of mass motion of the hapten will be slightly restricted and, hence, their contribution to the entropy may be somewhat underestimated. Because, however, nearly 100 (collective) degrees of freedom contribute significantly to the entropy, we consider this artifact negligible.

In summary, we assume that our entropy estimate can serve as a lower limit for the true entropic contribution to the unbinding free energy landscape.

Enforced unbinding for two ANO2 mutants

As already discussed, certain residues of the ANO2 binding pocket strongly interact with the hapten molecule (see, e.g., Fig. 12). Particularly strong bonds are formed to the light chain residues, and mutations of those affect the ANO2/DNP-hapten binding free energy (Martinez-Yamout and McConnell, 1994). In this section we ask whether such mutations can also alter the unbinding force. To that end, the two critical residues shown in Fig. 15, Tyr-33(L) (green) and Ile-96(L) (red), were chosen as mutation sites, and the respective mutant structures of the ANO2 antibody were modeled and subjected to FPMD simulations.

In the first mutant, Y33F(L), the strong hydrogen bond between the hydroxyl group of Tyr-33(L) and the amino group (N8,H29) of DNP-hapten was deleted by replacing the tyrosine with a phenylalanine. Accordingly, decreased unbinding forces for that mutant were expected. With the second mutant, I96K(L), we aimed at an increased unbinding force as compared to the wild-type complex. To this end, Ile-96(L) was replaced by a lysine that was expected to

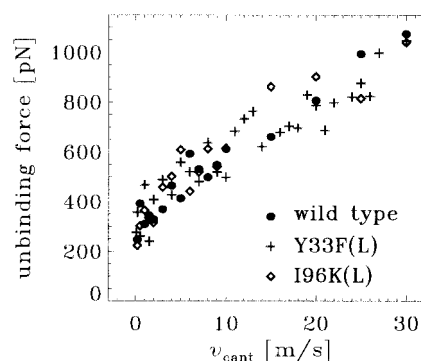


FIGURE 16 Unbinding forces of the ANO2/DNP-hapten complex as a function of pulling velocity for the wild type (●), the Y33F(L) mutant (+), and the I96K(L) mutant (◇).

form an additional hydrogen bond to the oxygen atom O25 of the DNP ring.

Modeling of these two mutants was performed as described in the Methods section. No severe structural distortions were expected because the two mutations did not induce steric strain into the structure of the binding pocket. This was checked by monitoring the rms deviation of the binding pocket from the wild-type x-ray structure during equilibration as well as the interactions between hapten and the remaining binding pocket residues (data not shown). Indeed, none of these observables differs significantly from those monitored during equilibration of the wild type. We therefore assume that our models of the two mutants are accurate.

Starting from the respective equilibrated structures, 22 FPMD simulations per mutant were carried out using pulling velocities between 2 and 50 m/s. Fig. 16 compares the obtained unbinding forces with those obtained for the wild type. Unbinding forces for the wild-type complex (●), the Y33F(L) mutant (+), and the I96K(L) mutant (◇), respectively, are plotted as a function of pulling velocity v_{cant} .

Surprisingly, no significant difference for the calculated unbinding forces is seen. After rescaling the computed unbinding forces to typical experimental time scales (Heymann and Grubmüller, 1999a), we obtain 68 ± 25 pN for the Y33F(L) mutant and 73 ± 20 pN for the I96K(L) mutant, which is to be compared with the unbinding force of 65 ± 25 pN for the wild-type complex (Heymann and Grubmüller, 1999a). For rescaling, a dissociation constant of $k = 110 \text{ s}^{-1}$ was used for all three cases because that quantity only weakly affects the results.

For an explanation for this result, first consider the snapshots in Fig. 17, which show the binding pocket of the Y33F(L) mutant and the bound hapten (gray) after equilibration (top) and at $z_{\text{cant}} = 4 \text{ Å}$ (bottom); the removed hydrogen bond is tagged with a cross. That hydrogen bond, however, is subsequently fully restored by Tyr-31(L) which, as can be seen in the bottom snapshot, is close to Phe-33(L)

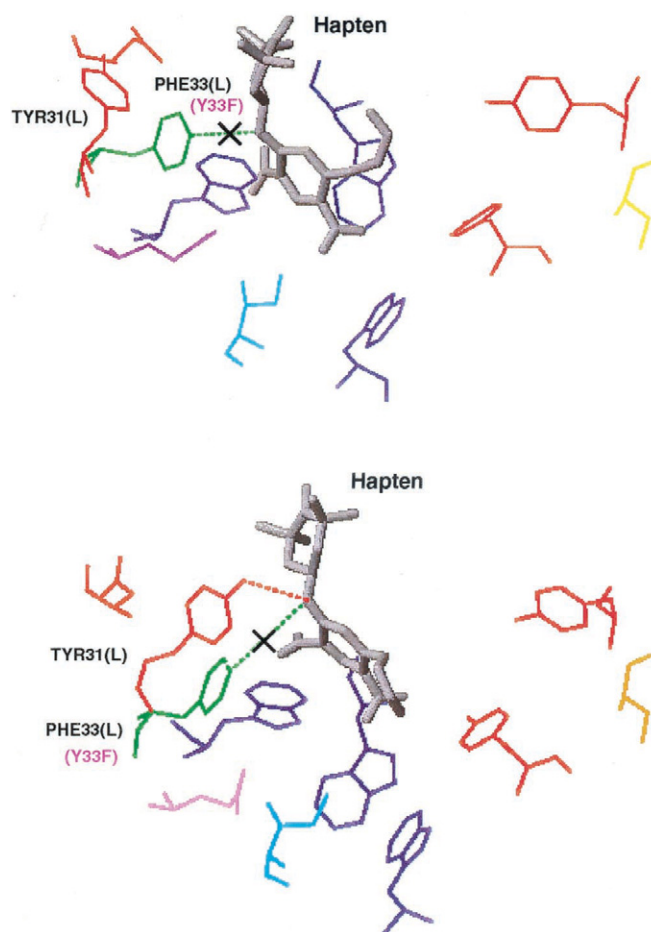


FIGURE 17 Snapshots of the binding pocket during enforced unbinding for the Y33F(L) mutant. *Top*: bound state after equilibration; the removed hydrogen bond is indicated. *Bottom*: intermediate at $z_{\text{cant}} \approx 4 \text{ \AA}$. A newly formed hydrogen bond between hapten and Tyr-31(L) is shown by the dashed line.

and moves toward the hapten amino group during unbinding, thereby perfectly replacing the wild-type Tyr-33(L).

The energetics of this process is obtained from the interaction fingerprint shown in Fig. 18 (*top*). As intended, the Phe-33(L) bond to the hapten is weakened to a large extent with respect to the Tyr-33(L) interactions in the wild type (cf. also Fig. 12). As described above, subsequently pronounced interactions between Tyr-31(L) and hapten build up for $z_{\text{cant}} > 4 \text{ \AA}$ and reach their maximum in the range between 6 and 8 \AA . Additionally, and possibly triggered by the motion of Tyr-31(L), a strong bond is formed to Asp-49(L). In line with this finding, mutations of Asp-49(L), e.g., D50T(L) and D50S(L), also show changed binding constants (Martinez-Yamout and McConnell, 1994).

Both bonds contribute to the total interaction energy, which in this region is even larger than it is after equilibration. As a result, the corresponding force profile (Fig. 18, *bottom*) exhibits a second barrier in this part of the unbinding process. In many of the simulations, this barrier was

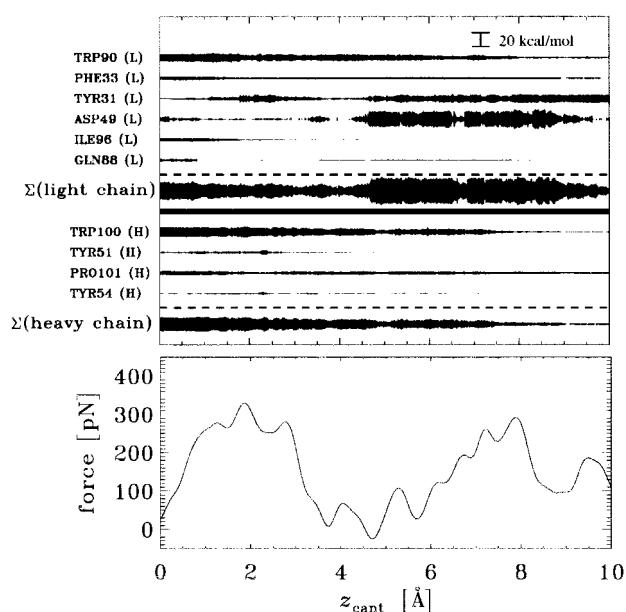


FIGURE 18 Interaction fingerprints (*top*) and force profile (*bottom*) for an FPMD simulation of the Y33F(L) mutant with $v_{\text{cant}} = 1 \text{ m/s}$.

similar in size to the first barrier; in several of the FPMD simulations the second barrier even dominated the first barrier and thus determined the unbinding force. To enable such a tyrosine swap, the binding pocket region must obviously be highly flexible.

For the I96K(L) mutant, the fingerprint for a typical FPMD probe simulation (Fig. 19, *top*) confirms the intended new strong interaction between the Lys-96(L) and hapten. Apparently, this interaction is indeed very stable, as it is

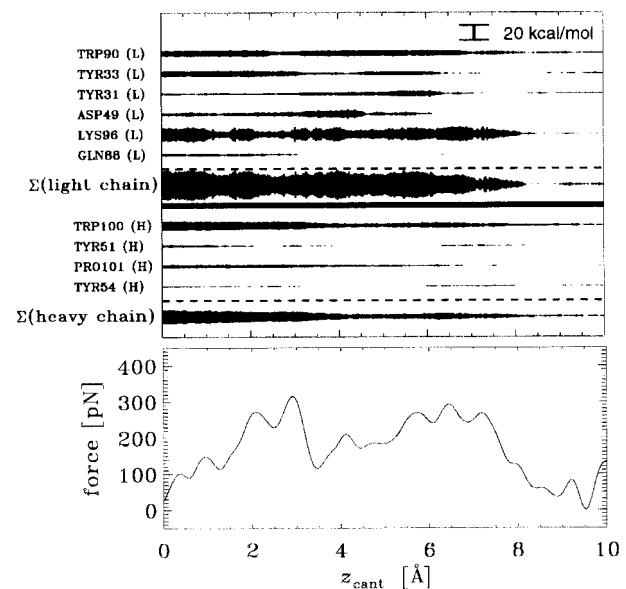


FIGURE 19 Interaction fingerprint (*top*) and force profile (*bottom*) of the I96K(L) mutant for an FPMD simulation with $v_{\text{cant}} = 1 \text{ m/s}$.

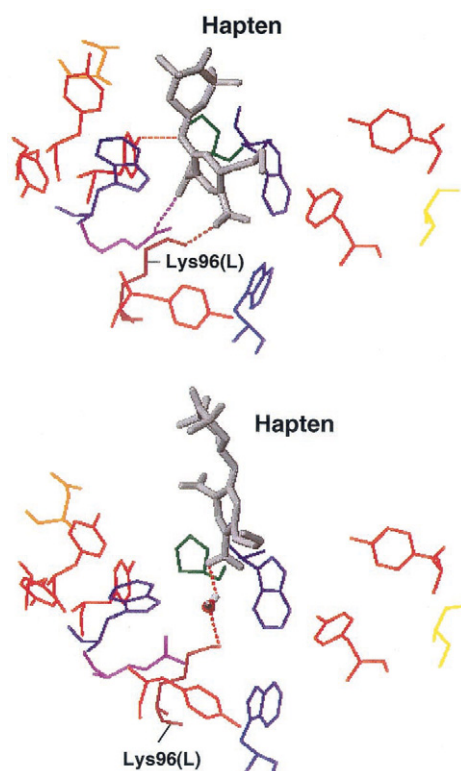


FIGURE 20 Snapshots of the binding pocket during enforced unbinding of the 196K(L) mutant complex. *Top*: bound state after equilibration. *Bottom*: Intermediate at $z_{\text{cant}} \approx 8$ Å. Also shown is a water molecule that forms a water bridge between Lys-96(L) and the haptene molecule.

almost unchanged for a long period during enforced unbinding, until $z_{\text{cant}} \approx 8$ Å. The force profile (*bottom*), however, does not exhibit higher maxima than the wild-type force profiles. Instead, the maximum *broadens* and the average force in this part of the pathway is larger without affecting the unbinding force.

The strong and long-lasting interaction to Lys-96(L) is explained in Fig. 20. After equilibration (*top*), the side chain of Lys-96(L) interacts with the oxygen atom O25 of the DNP ring (*dashed line*), which was the rationale for considering that mutant. Compared to the wild-type isoleucine, however, the lysine side chain turned out to be significantly more flexible. It was therefore dragged by the haptene molecule during the first unbinding steps and moved toward the binding pocket exit. As a consequence, the interactions between haptene and Lys-96(L) stayed essentially intact for an extended period, as already was evident from the interaction fingerprint. Furthermore, after rupture of that hydrogen bond (*bottom* of Fig. 20), a water molecule (also shown in the bottom snapshot) moved in between the haptene and Lys-96(L) and formed a transient water bridge. At this instance, although the haptene DNP ring had already been released from the tryptophan sandwich, the equilibrium interaction network was still partly in place. It is this slower breakdown of this interaction network, as compared to the

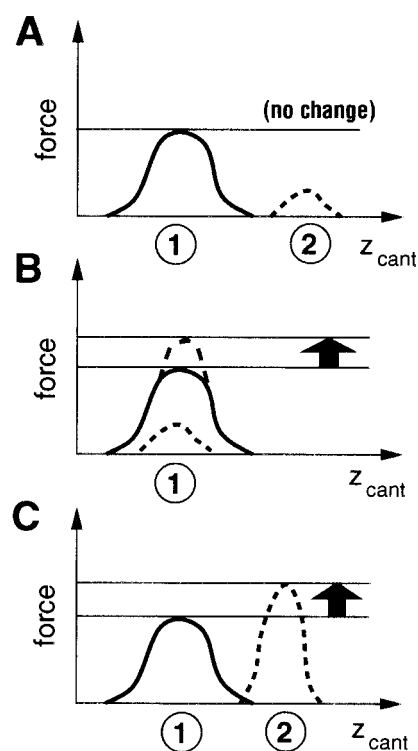


FIGURE 21 Modification of individual interactions may or may not affect the unbinding force, depending on the part of the reaction pathway at which they take place. See text for discussion.

wild type, that causes the barrier in the force profile to become broader rather than higher, again leaving the unbinding force essentially unchanged.

Viewed from a more general angle, the fact that no change of unbinding forces is seen in the above two mutation studies—whereas binding free energies do change—is probably less surprising, as it may appear at first sight. Note that, because free energies are thermodynamic state variables, free energy differences always add up to zero in a thermodynamic cycle. Therefore, to estimate the effect of a mutant on the binding free energy, it suffices to consider its effect on the bound state, i.e., how much the interaction free energy with the ligand is altered, e.g., due to removal of a single hydrogen bond. Accordingly, the binding free energy is independent of the unbinding pathway. Vice versa, no information on the unbinding pathway can be extracted from binding free energies.

As illustrated in Fig. 21, the situation is more complex for unbinding forces. Here, mutations or other changes may or may not affect the unbinding force, depending on how large their effect is and depending on which part of the reaction pathway is affected. Panel *A* illustrates one of the many possibilities for which a mutation will not affect the unbinding force. That force is generally determined by the maximum in the force profile (*solid line*), here at position ①. The change induced at position ② (*dashed line*), unless large,

will not affect the unbinding force. In contrast, the binding free energy, obtained from the integral over the force profile, will obviously be raised.

Only two possibilities remain for which the unbinding force is actually affected. First (*B*), a mutation that causes an additional force component (*dashed lines*) right within part ① of the pathway that contains the force maximum, will affect the unbinding force in a way similar to its effect on the binding free energy. Second (*C*), an additional force component that, although at a different position ② is large enough to exceed the force maximum, will also show up. Neither of these two cases is realized for the two mutants described above, and therefore no effect is seen.

In the above sense, binding forces are affected by changes of the binding pocket in a *nonadditive* way, and prediction of the effect requires analysis not only of the bound state, but also of the whole unbinding pathway. Vice versa, force probe mutation studies can therefore provide additional information on the reaction pathway.

We note that cases (*B*) and (*C*) can be distinguished experimentally by dynamic force spectroscopy where the pulling velocity is varied. Thereby, the position of the force maximum can be determined (Evans and Ritchie, 1997; Merkel et al., 1999), and additional information about the shape of the force profile can be obtained (Heymann and Grubmüller, 2000).

CONCLUSIONS

Extended force probe molecular dynamics (FPMD) simulations of a solvated AN02/DNP-hapten complex have been carried out, and the unbinding pathways of the hapten molecule out of the AN02 binding pocket were analyzed. Two phases, A and B of the unbinding process, were seen. During phase A, the hapten molecule is released from the rigid tryptophan sandwich. Structural and energetic details of this part of the unbinding pathway are well-defined and were reproduced in all simulations. In contrast, phase B, which begins approximately at the force maximum and well after release of the hapten from the tryptophan sandwich, is characterized by significant structural heterogeneity of the unbinding pathways. As two extreme cases, a “light chain route” and a “heavy chain route” have been described.

Which of the two routes is taken in phase B is already remarkably predetermined to a high degree in phase A. Here, the hydrogen bond to Tyr-33(L) acts as a switch and the timing of breakage of that particular hydrogen bond with respect to the release from the tryptophan sandwich turned out to be critical. These findings provide a microscopic model for the structural heterogeneity found in NMR studies (Martinez-Yamout and McConnell, 1994).

The large number of FPMD simulations carried out enabled us to estimate the entropic contribution to the binding free energy that results from the observed heterogeneity of the unbinding pathways. Our approach to compute entropy

curves along reaction pathways from ensembles of *trajectories* is a straightforward generalization of the established methods to estimate free energy values or differences from ensembles of *structures*. The underlying change of view—from thermodynamic states to reaction pathways—was in fact motivated by the corresponding new perspective—from energies to forces—provided by force probe experiments.

We note that our entropy estimate refers to *enforced* unbinding pathways, as observed in AFM experiments and in our force probe simulations, rather than to spontaneous unbinding pathways. However, because the configurational space accessible to the hapten during *free* unbinding is equal to or larger than that for directed unbinding, the entropic contribution to the free energy along the *spontaneous* unbinding pathway is presumably even larger than (or at least not smaller than) the estimate provided here.

The obtained entropic contribution to the binding free energy barrier of 6 kcal/mol, which we thus consider a lower limit, is substantial and contributes ~40% to the binding free energy of 15 kcal/mol. Thus it seems safe to say that for the AN02/DNP-hapten complex, the activation free energy barrier is significantly lower than the enthalpic barrier. Accordingly, the binding kinetics is modified by an entropic contribution that involves a large number of degrees of freedom both of the DNP ligand and that of the antibody. In particular, as can be seen from inspection of the PCA eigenvectors (data not shown), these degrees of freedom are not localized at the binding pocket, and they also involve residues up to 15 Å apart. This result provides an explanation for the recent finding that mutations of residues at that distance from the binding pocket can indeed affect the AN02 binding kinetics (Wedemayer et al., 1997). Our results also suggest that, more generally, induced fit motions like those seen, e.g., for Tyr-31(L) can, through entropic effects, significantly change the binding kinetics.

Within this context one may speculate about the physiological role of the entropic modification of barrier heights and binding kinetics. We think that such “entropic control” provides a means to compensate for the enthalpic contribution to binding free energy barriers. This enthalpic contribution can certainly not be fully adjusted only by variation of the binding pocket due to the huge diversity of antigens that have to be bound. However, there is obviously an optimal value for the binding kinetics: if, for example, the off-rate were too low, only a few antigens can be bound; if it were too fast, binding events might not be recognized. Here, entropic control could, via adjustment of the flexibility of the binding pocket, tailor the binding energy profile appropriately.

For the initial steps of antigen binding, the “fan” of binding pathways most likely provides a means to enhance the efficiency of antigen binding: because here many configurations ultimately lead down the “binding funnel” toward the fully bound state, proper pre-orientation of the antigen is presumably not required, and the rate of success-

ful first encounters is thereby enhanced. The obvious similarity to the concept of a protein “folding funnel” (Wolynes et al., 1995), which has been pointed out previously (Rejto and Verkhivker, 1996; Kumar et al., 2000), suggests that the antibody/antigen system, being computationally more easily accessible than protein folding, may serve as a model system for future studies of the “funnel” concept.

Our FPMD simulations of the mutated complexes revealed two interesting mechanisms. First, as seen for the Y33F(L) mutant, the function of a modified residue can be adopted by another residue such that the binding force is essentially unchanged. Second, our results suggest that binding forces are generally nonadditive with respect to the underlying individual interatomic interactions like hydrogen bonds or van der Waals contacts. In particular, adding a new interaction through site-directed mutations does not necessarily increase the binding force even if the binding free energy is raised.

The authors thank Bert de Groot and Jaydev Jethwa for carefully reading the manuscript and Rainer Böckmann and Bert de Groot for help with the programs DynDom and alicut.

This work was supported by the Deutsche Forschungsgemeinschaft (Grants Gr 1590/1-1 and Gr 1590/1-2).

REFERENCES

- Allen, S., X. Chen, J. Davies, M. Davies, A. C. Dawkes, J. C. Edwards, C. J. Roberts, J. Sefton, S. J. B. Tendler, and P. M. Williams. 1997. Detection of antigen-antibody binding events with atomic force microscope. *Biochemistry*. 36:7457–7463.
- Amadei, A., A. B. M. Linssen, and H. J. C. Berendsen. 1993. Essential dynamics of proteins. *Proteins*. 17:412–425.
- Anglister, J., M. W. Bond, T. Frey, D. Leahy, M. Levitt, H. M. McConnell, G. S. Rule, J. Tomasello, and M. Whittake. 1987. Contribution of tryptophan residues to the combining site of a monoclonal anti-dinitrophenyl spin-label antibody. *Biochemistry*. 26:6058–6064.
- Ansari, A., J. Berendsen, S. F. Browne, H. Frauenfelder, I. E. T. Iben, T. B. Sauke, E. Shyamsunder, and R. D. Young. 1985. Protein states and protein quakes. *Proc. Natl. Acad. Sci. U.S.A.* 82:5000–5004.
- Bell, G. I. 1978. Models for the specific adhesion of cells to cell. *Science*. 200:618–627.
- Berendsen, H. J. C., J. P. M. Postma, W. F. van Gunsteren, A. Dinola, and J. R. Haak. 1984. Molecular dynamics with coupling to an external bath. *J. Chem. Phys.* 81:3684–3690.
- Bernstein, F. C., T. F. Koetzle, G. J. B. Williams, E. F. Meyer, M. D. Brice, J. R. Rodgers, O. Kennard, T. Shimanouchi, and M. J. Tasumi. 1977. The protein data bank: a computer-based archival file for molecular structures. *J. Mol. Biol.* 112:535–542.
- Brooks, B. R., R. E. Bruccoleri, B. D. Olafson, D. J. States, S. Swaminathan, and M. Karplus. 1983. CHARMM: a program for macromolecular energy, minimization, and dynamics calculations. *J. Comput. Chem.* 4:187–217.
- Brooks III, C. L., and M. Karplus. 1983. Deformable stochastic boundaries in molecular dynamics. *J. Chem. Phys.* 79:6312–6325.
- Brünger, A. T. 1988. X-PLOR. The Howard Hughes Medical Institute and Department of Molecular Biophysics and Biochemistry, Yale University, 260 Whitney Avenue, P.O. Box 6666, New Haven, CT 06511.
- Brünger, A. T., D. J. Leahy, T. R. Hynes, and R. O. Fox. 1991. 2.9 Å resolution structure of an anti-dinitrophenyl-spin-label monoclonal antibody F_{ab} fragment with bound hapten. *J. Mol. Biol.* 221:239–256.
- Dammer, U., M. Hegner, D. Anselmetti, P. Wagner, M. Dreier, W. Huber, and H.-J. Güntherodt. 1996. Specific antigen/antibody interactions measured by force microscopy. *Biophys. J.* 70:2437–2441.
- Dickman, S. 1998. Antibodies stage a comeback in cancer treatment. *Science*. 280:1196–1197.
- Eichinger, M., H. Grubmüller, H. Heller, and P. Tavan. 1997. FAMUSAMM: a new algorithm for rapid evaluation of electrostatic interaction in molecular dynamics simulations. *J. Chem. Phys.* 18:1729–1749.
- Eichinger, M., H. Heller, and H. Grubmüller. 2000. EGO: an efficient molecular dynamics program and its application to protein dynamics simulations. In *Workshop on Molecular Dynamics on Parallel Computers*, John von Neumann Institute for Computing (NIC) Research Centre. R. Esser, P. Grassberger, J. Grotendorst, and M. Lewerenz, editors. World Scientific, Jülich, Germany. 154–174.
- Elber, R., and M. Karplus. 1987. Multiple conformational states of proteins: a molecular dynamics analysis of myoglobin. *Science*. 235:318–321.
- Evans, E., and K. Ritchie. 1997. Dynamic strength of molecular adhesion bonds. *Biophys. J.* 72:1541–1555.
- Eyring, H. J. 1935. The activated complex in chemical reactions. *J. Chem. Phys.* 3:107–115.
- Florin, E.-L., V. T. Moy, and H. E. Gaub. 1994. Adhesion forces between individual ligand-receptor pairs. *Science*. 264:415–417.
- Frauenfelder, H., P. J. Steinbach, and R. D. Young. 1989. Conformational relaxation in proteins. *Chem. Ser.* 29:145–150a. (Abstr.)
- García, A. E. 1992. Large-amplitude nonlinear motions in proteins. *Phys. Rev. Lett.* 68:2696–2699.
- Gardiner, C. W. 1985. *Handbook of Stochastic Methods*. Springer-Verlag, Berlin, Heidelberg, New York.
- Grubmüller, H. 1995. Predicting slow structural transitions in macromolecular systems: Conformational flooding. *Phys. Rev. E*. 52:2893–2906.
- Grubmüller, H., B. Heymann, and P. Tavan. 1996. Ligand binding: molecular mechanics calculation of the streptavidin-biotin rupture force. *Science*. 271:997–999.
- Grubmüller, H., and P. Tavan. 1998. Multiple time step algorithms for molecular dynamics simulations of proteins: how good are they? *J. Comput. Chem.* 19:1534–1552.
- Hayward, S., and H. J. C. Berendsen. 1998. Systematic analysis of domain motions in proteins from conformational change: new results on citrate synthase and T4 lysozyme. *Proteins*. 30:144–154.
- Heymann, B., and H. Grubmüller. 1999a. AN02/DNP unbinding forces studied by molecular dynamics AFM simulations. *Chem. Phys. Lett.* 303:1–9.
- Heymann, B., and H. Grubmüller. 1999b. “Chair-boat” transitions and side groups affect the stiffness of polysaccharides. *Chem. Phys. Lett.* 305:202–208.
- Heymann, B., and H. Grubmüller. 1999c. Elastic properties of poly(ethylene glycol) studied by molecular dynamics stretching simulations. *Chem. Phys. Lett.* 307:425–432.
- Heymann, B., and H. Grubmüller. 2000. Dynamic force spectroscopy of molecular adhesion bonds. *Phys. Rev. Lett.* 84:6126–6129.
- Hinterdorfer, P., W. Baumgartner, H. J. Gruber, K. Schlicher, and H. Schindler. 1996. Detection and localization of individual antibody-antigen recognition events by atomic force microscopy. *Proc. Natl. Acad. Sci. U.S.A.* 93:3477–3481.
- Israelowitz, B., S. Izrailev, and K. Schulten. 1997. Binding pathway of retinal to bacterio-opsin: a prediction by molecular dynamics simulations. *Biophys. J.* 73:2972–2979.
- Izrailev, S., S. Stepaniants, M. Balsera, Y. Oono, and K. Schulten. 1997. Molecular dynamics study of unbinding of the avidin-biotin complex. *Biophys. J.* 72:1568–1581.
- Jorgensen, W. L., J. Chandrasekhar, and J. D. Madura. 1983. Comparison of simple potential functions for simulating liquid water. *J. Chem. Phys.* 79:926–935.
- Karplus, M., and J. N. Kushick. 1981. Method for estimating the configurational entropy of macromolecules. *Macromolecules*. 14:325–332.

- Kellermayer, M. S. Z., S. B. Smith, H. L. Granzier, and C. Bustamante. 1997. Folding-unfolding transitions in single titin molecules characterized with laser tweezers. *Science*. 276:1112–1116.
- Kitao, A., F. Hirata, and N. Go. 1991. The effects of solvent on the conformation and the collective motions of a protein: normal mode analysis and molecular dynamics simulations of melittin in water and in vacuum. *J. Phys. Chem.* 158:447–472.
- Kitao, A., F. Hirata, and N. Go. 1993. Effects of solvent on the conformation and the collective motions of a protein. 2. Structure of hydration in melittin. *J. Phys. Chem.* 97:10223–10230.
- Konrad, M. W., and J. I. Bolonick. 1996. Simulation of DNA stretching. *J. Am. Chem. Soc.* 118:10986–10994.
- Koradi, R., M. Billeter, and K. Wüthrich. 1996. MOLMOL: a program for display and analysis of macromolecular structures. *J. Mol. Graphics.* 14:51–55.
- Kossmann, R. 1997. Entwicklung eines effektiven Randpotentials für Molekulardynamik-simulationen wässriger Lösungen. Master's thesis, Ludwig-Maximilians-Universität München.
- Kramers, H. A. 1940. Brownian motion in a field of force and the diffusion model of chemical reactions. *Physica (Utrecht)*. VII:284–304.
- Kraulis, P. J. 1991. Molscript: a program to produce both detailed and schematic plots of protein structures. *J. Appl. Crystallogr.* 24:946–950.
- Kristensen, O., D. G. Vassilyev, F. Tanaka, K. Morikawa, and I. Fujii. 1998. A structural basis for transition-state stabilization in antibody-catalyzed hydrolysis: crystal structures of an abzyme at 1.8 Å resolution. *J. Mol. Biol.* 281:501–511.
- Kumar, S., B. Y. Ma, C. J. Tsai, N. Sinha, and R. Nussinov. 2000. Folding and binding cascades: dynamic landscapes and population shifts. *Protein Sci.* 9:10–19.
- Leahy, D. J., G. S. Rule, M. M. Whittaker, and H. M. McConnell. 1988. Sequences of 12 monoclonal anti-dinitrophenyl spin-label antibodies for NMR studies. *Proc. Natl. Acad. Sci. U.S.A.* 85:3661–3665.
- Lee, G. U., L. A. Chrisey, and R. J. Colton. 1994a. Direct measurement of the forces between complementary strands of DNA. *Science*. 266:771–773.
- Lee, G. U., D. A. Kidwell, and R. J. Colton. 1994b. Sensing discrete streptavidin-biotin interactions with atomic force microscopy. *Langmuir*. 10:354–357.
- Lu, H., B. Israelewitz, A. Krammer, V. Vogel, and K. Schulten. 1998. Unfolding of titin immunoglobulin domains by steered molecular dynamics simulation. *Biophys. J.* 75:662–671.
- Mardia, K. V., J. T. Kent, and J. M. Bibby. 1979. *Multivariate Analysis*. Academic Press, London.
- Marrink, S., O. Berger, P. Tieleman, and F. Jähnig. 1998. Adhesion forces of lipids in a phospholipid membrane studied by molecular dynamics simulations. *Biophys. J.* 74:931–943.
- Martinez-Yamout, M., and H. M. McConnell. 1994. Site-directed mutagenesis and ¹H nuclear magnetic resonance of anti-dinitrophenyl spin label antibody. *J. Mol. Biol.* 244:301–318.
- McCammon, J. A., B. R. Gelin, and M. Karplus. 1977. Dynamics of folded proteins. *Nature (Lond.)*. 267:585–590.
- McConnell, H. M., and M. Martinez-Yamout. 1996. Insight into antibody combining sites using nuclear magnetic resonance and spin label hap- tens. *Adv. Protein Chem.* 49:135–149.
- Merkel, R., P. Nassoy, A. Leung, K. Ritchie, and E. Evans. 1999. Energy landscapes of receptor-ligand bonds explored with dynamic force spectroscopy. *Nature (Lond.)*. 397:50–53.
- Molecular Simulations Inc. 1997. *QUANTA Basic Operations*. San Diego, CA.
- Moy, V. T., E.-L. Florin, and H. E. Gaub. 1994. Intermolecular forces and energies between ligands and receptors. *Science*. 266:257–258.
- Murzin, A. G., S. E. Brenner, T. Hubbard, and C. Chothia. 1995. SCOP: a structural classification of protein databases for the investigation of sequences and structures. *J. Mol. Biol.* 247:536–540.
- Padlan, E. A. 1994. Anatomy of the antibody molecule. *Mol. Immunol.* 31:169–217.
- Reif, F. 1965. *Fundamentals of Statistical Mechanics*. McGraw-Hill Book Company, San Francisco.
- Rejto, P. A., and G. M. Verkhivker. 1996. Unraveling principles of lead discovery: from unfrustrated energy landscapes to novel molecular anchors. *Proc. Natl. Acad. Sci. U.S.A.* 93:8945–8950.
- Rief, M., M. Gautel, F. Oesterhelt, J. M. Fernandez, and H. E. Gaub. 1997a. Reversible unfolding of individual titin Ig-domains by AFM. *Science*. 276:1109–1112.
- Rief, M., F. Oesterhelt, B. Heymann, and H. E. Gaub. 1997b. Single molecule force spectroscopy reveals conformational change in polysaccharides. *Science*. 275:1295–1297.
- Ros, R., F. Schwesinger, D. Anselmetti, M. Kubon, R. Schäfer, A. Plückthun, and L. Tiefenauer. 1998. Antigen binding forces of individually addressed single-chain F_v antibody molecules. *Proc. Natl. Acad. Sci. U.S.A.* 95:7402–7405.
- Schlitter, J. 1993. Estimation of absolute and relative entropies of macromolecules using the covariance matrix. *Chem. Phys. Lett.* 215:617–621.
- Schulze, B. G., H. Grubmüller, and J. D. Evanseck. 2000. Functional significance of hierarchical tiers in carbonmonoxy myoglobin: conformational substates and transitions studied by conformational flooding simulations. *J. Am. Chem. Soc.* 122:8700–8711.
- Stella, L., and S. Melchionna. 1998. Equilibration and sampling in molecular dynamics simulations of biomolecules. *J. Chem. Phys.* 109:10115–10117.
- Theriault, T. P., D. J. Leahy, M. L. Levitt, H. M. McConnell, and G. S. Rule. 1991. Structural and kinetic studies of the F_{ab} fragment of a monoclonal anti-spin label antibody by nuclear magnetic resonance. *J. Mol. Biol.* 221:257–270.
- Theriault, T. P., H. M. McConnell, A. K. Singhal, and G. S. Rule. 1993. Anomalous kinetics in antibody-antigen interactions. *J. Phys. Chem.* 97:3034–3039.
- Tskhovrebova, L., J. Trinck, J. A. Sleep, and R. M. Simmons. 1997. Elasticity and unfolding of single molecules of the giant muscle protein titin. *Nature (Lond.)*. 387:308–312.
- Van Aalten, D. M. F., D. A. Conn, B. L. De Groot, J. B. C. Findlay, H. J. C. Berendsen, and A. Amadei. 1997. Protein dynamics derived from clusters of crystal structures. *Biophys. J.* 73:2891–2896.
- Wedemayer, G. J., P. A. Patten, L. H. Wang, P. G. Schultz, and R. C. Stevens. 1997. Structural insights into the evolution of an antibody combining site. *Science*. 276:1665–1669.
- Wolynes, P. G., J. N. Onuchic, and D. Thirumalai. 1995. Navigating the folding routes. *Science*. 267:1619–1620.